Published OnlineFirst December 11, 2019; DOI: 10.1158/2159-8290.CD-19-0569

RESEARCH ARTICLE

MAIT Cells Promote Tumor Initiation, Growth, and Metastases via Tumor MR1

Juming Yan[1,2], Stacey Allen[1], Elizabeth McDonald[1], Indrajit Das[3], Jeffrey Y.W. Mak[4,5], Ligong Liu[4,5], David P. Fairlie[4,5], Bronwyn S. Meehan[6], Zhenjun Chen[6], Alexandra J. Corbett[6], Antiopi Varelias[2,7], Mark J. Smyth[2,3], and Michele W.L. Teng[1,2]

Published OnlineFirst December 11, 2019; DOI: 10.1158/2159-8290.CD-19-0569

ABSTRACT

Mucosal-associated invariant T (MAIT) cells are innate-like T cells that require MHC class I–related protein 1 (MR1) for their development. The role of MAIT cells in cancer is unclear, and to date no study has evaluated these cells *in vivo* in this context. Here, we demonstrated that tumor initiation, growth, and experimental lung metastasis were significantly reduced in *Mr1*$^{-/-}$ mice, compared with wild-type mice. The antitumor activity observed in *Mr1*$^{-/-}$ mice required natural killer (NK) and/or CD8$^+$ T cells and IFNγ. Adoptive transfer of MAIT cells into *Mr1*$^{-/-}$ mice reversed metastasis reduction. Similarly, MR1-blocking antibodies decreased lung metastases and suppressed tumor growth. Following MR1 ligand exposure, some, but not all, mouse and human tumor cell lines upregulated MR1. Pretreatment of tumor cells with the stimulatory ligand 5-OP-RU or inhibitory ligand Ac-6-FP increased or decreased lung metastases, respectively. MR1-deleted tumors resulted in fewer metastases compared with parental tumor cells. MAIT cell suppression of NK-cell effector function was tumor-MR1–dependent and partially required IL17A. Our studies indicate that MAIT cells display tumor-promoting function by suppressing T and/or NK cells and that blocking MR1 may represent a new therapeutic strategy for cancer immunotherapy.

SIGNIFICANCE: Contradicting the perception that MAIT cells kill tumor cells, here MAIT cells promoted tumor initiation, growth, and metastasis. MR1-expressing tumor cells activated MAIT cells to reduce NK-cell effector function, partly in a host IL17A–dependent manner. MR1-blocking antibodies reduced tumor metastases and growth, and may represent a new class of cancer therapeutics.

INTRODUCTION

The tumor microenvironment (TME) contains various immune cells that can promote or suppress tumor growth (1). Conventional αβ$^+$ CD8$^+$ T cells, which recognize peptide antigens in the context of MHC class I, are key in mediating antitumor responses and thought to be the main cells targeted by current immune-checkpoint inhibitors. However, there is now a growing appreciation that unconventional innate-like T cells, which do not recognize classic peptide antigens, can also be important in regulating tumor immunity, including γδ T cells, natural killer (NK) T cells, and mucosal-associated invariant T (MAIT) cells (reviewed in ref. 2).

MAIT cells are developmentally and functionally dependent on the MHC class I–related protein 1 (MR1) and the host microbiota (3–5). Unlike classic MHC molecules, MR1 presents microbial-derived metabolites to MAIT cells and is evolutionarily conserved across mammals, suggesting the importance of the MAIT TCR–MR1 axis in immunity (6). MR1 presents microbial-derived metabolites that can activate or inhibit MAIT cells (7–9). To date, 5-(2-oxopropylideneamino)-6-D-ribitylaminouracil (5-OP-RU), an adduct of a key riboflavin (vitamin B2) biosynthesis pathway intermediate (5-A-RU) and a glycolysis pathway intermediate (pyruvaldehyde), is the most potent stimulatory MAIT cell antigen (7, 8). In contrast, folate (vitamin B9)-based MR1 ligands such as 6-formyl pterin (6-FP) and its derivative acetyl 6-formylpterin (Ac-6-FP) inhibit MAIT cell activation (9–12). It has also been reported that other aromatic molecules including drugs, drug metabolites, and drug-like molecules (e.g., salicylates, diclofenac and its metabolite) acted as MR1-binding ligands that inhibited or activated MAIT cells (12). In the context of microbial infection, activation of MAIT cells through MR1–TCR engagement results in the rapid secretion of various cytokines including IFNγ, TNF, and IL17A (7, 9, 11, 13–18). Alternatively, MAIT cells can be activated in an MR1-independent, cytokine-dependent manner (18–22).

In mice, MAIT cells are generally low in frequency, although they are enriched in mucosal sites such as the lungs, liver, and intestine (18, 23, 24). In contrast, they are more abundant in humans, representing on average approximately 5% of total blood T cells, 10% of CD8$^+$ T cells, and up to 45% of liver T cells (15–17). The majority of mouse MAIT cells are CD4 and CD8 double-negative, although the frequency of MAIT cell subsets varies in a tissue- and strain-specific manner (18, 25). In contrast, most human MAIT cells are CD8 single-positive (17, 25, 26) and potentially may be erroneously identified as conventional CD8$^+$ T cells based on an assessment of CD8 positivity alone (e.g., in IHC and standard flow cytometry).

[1]Cancer Immunoregulation and Immunotherapy Laboratory, QIMR Berghofer Medical Research Institute, Herston, Australia. [2]School of Medicine, University of Queensland, Herston, Australia. [3]Immunology in Cancer and Infection Laboratory, QIMR Berghofer Medical Research Institute, Herston, Australia. [4]Division of Chemistry and Structural Biology, Institute for Molecular Bioscience, The University of Queensland, Brisbane, Australia. [5]ARC Centre of Excellence in Advanced Molecular Imaging, University of Queensland, Brisbane, Australia. [6]Department of Microbiology and Immunology, The University of Melbourne, The Peter Doherty Institute for Infection and Immunity, Victoria, Australia. [7]Transplantation Immunology Laboratory, QIMR Berghofer Medical Research Institute, Brisbane, Australia.

Note: Supplementary data for this article are available at Cancer Discovery Online (http://cancerdiscovery.aacrjournals.org/).

Corresponding Author: Michele W.L. Teng, QIMR Berghofer Medical Research Institute, 300 Herston Road, Brisbane, Queensland 4006, Australia. Phone: 617-3845-3958; Fax: 617-3362-0111; E-mail: michele.teng@qimrberghofer.edu.au

Cancer Discov 2020;10:124–41

doi: 10.1158/2159-8290.CD-19-0569

Published OnlineFirst December 11, 2019; DOI: 10.1158/2159-8290.CD-19-0569

Although MAIT cells were previously defined by the coexpression of various cell-surface markers and/or transcription factors, with the development of MR1–Ag tetramers (7, 17), they can now be definitively identified.

MAIT cells have been reported to have either protective or pathogenic roles in bacterial and fungal infection (27); however, their role in antitumor immunity is unknown. Clinically, a number of studies have reported that MAIT cells were present in different human tumors, including colorectal cancer (28–31), kidney and brain cancer (32), liver cancer (33), and multiple myeloma (34, 35). However, these studies identified MAIT cells by staining for TCRVα7.2, in combination with CD3 and CD161, except for the study by Gherardin and colleagues, where a human MR1 tetramer was used (34). In colorectal cancer, the frequency of MAIT cells was reported to be higher in cancer tissues compared with normal adjacent tissues (28–31). In one study, high levels of MAIT cell infiltration in colorectal tumors were associated with poor clinical outcome (29). In contrast, Shaler and colleagues reported that MAIT cell frequencies were lower in colorectal liver metastases compared with healthy liver tissues (36). Similarly, another study reported that MAIT cell frequencies decreased in hepatocellular carcinoma compared with healthy liver tissues and correlated with poor prognosis (33). In the bone marrow of patients with multiple myeloma, MAIT cell frequencies were found to be decreased compared with healthy controls (35). Currently, MAIT cells are proposed to have antitumor activity, because *in vitro* it was demonstrated that they displayed cytolytic activity against tumor cells when cultured at a high effector:target ratio in the presence of MAIT cell antigen or following PMA/ionomycin stimulation (30, 31, 34). Preclinically, the *in vivo* functional role of MAIT cells in promoting or suppressing antitumor immunity has not been demonstrated. In this study, we investigated the role of MAIT cells in tumor initiation and control of experimental lung metastases, subcutaneous tumor growth, and their mechanism of action.

RESULTS

Tumor Initiation, Growth, and Metastases Are Suppressed in *Mr1*$^{-/-}$ Mice

Critically, MAIT cell regulation of antitumor immunity has never been investigated *in vivo*. The role of MAIT cells in experimental tumor metastasis to the lung was investigated by comparing metastasis in C57BL/6 wild-type (WT) and C57BL/6 *Mr1*$^{-/-}$ mice, which lack MAIT cells (ref. 5; Fig. 1). Given that MAIT cells respond to microbial metabolites and the microbiota between WT and *Mr1*$^{-/-}$ mice was reported to be different (24), we first set up an experiment where we injected B16F10 melanoma cells intravenously into WT or *Mr1*$^{-/-}$ mice that were housed separately or cohoused for at least 4 weeks prior to injection. In both settings, the numbers of lung metastases were significantly reduced in *Mr1*$^{-/-}$ mice compared with WT mice, suggesting that MAIT cells promoted metastasis (Fig. 1A). This suggested the reduction in metastases was not due to differences in microbiota between WT and *Mr1*$^{-/-}$ mice. Nevertheless, to minimize any potential confounding effects of the microbiota on our experiments, cohoused WT and *Mr1*$^{-/-}$ mice were used in all the *in vivo* experiments performed in this study.

To confirm suppression of lung metastases occurred in another tumor model, we injected LWT1, a BRAF^{V600E}-mutant melanoma cell line, into WT and *Mr1*$^{-/-}$ mice (Fig. 1B). Again, the numbers of LWT1 metastases were significantly reduced in *Mr1*$^{-/-}$ mice compared with WT mice. Given the critical roles of NK cells and IFNγ in the control of experimental lung metastases (37), we next depleted NK cells or neutralized IFNγ in B16F10 tumor–bearing WT or *Mr1*$^{-/-}$ mice (Fig. 1C and D). Although control Ig (cIg)–treated tumor-bearing *Mr1*$^{-/-}$ mice had fewer lung metastases compared with cIg-treated WT mice, tumor-bearing WT and *Mr1*$^{-/-}$ mice depleted of NK cells or neutralized of IFNγ displayed a similar higher level of lung metastases. These results demonstrated that the reduced metastasis observed in *Mr1*$^{-/-}$ mice was critically dependent upon NK cells and IFNγ. To further demonstrate that loss of MAIT cells was responsible for the reduction in lung metastases, we generated four-way bone marrow (BM) chimeric mice from WT or *Mr1*$^{-/-}$ donors (Fig. 1E). BM reconstitution was confirmed in the recipient mice with engraftment efficiency greater than 95% and it was confirmed that MAIT cells were lacking in mice transferred with *Mr1*$^{-/-}$ BM (data not shown). Only mice reconstituted with *Mr1*$^{-/-}$ BM displayed reduced tumor metastases (Fig. 1E), suggesting that loss of hematopoietic MR1 (and MAIT cell loss) contributed to lung metastasis suppression in *Mr1*$^{-/-}$ mice. In addition to experimental lung metastases, NK cells are also critical for protecting the host from methylcholanthrene (MCA) carcinogen–induced fibrosarcoma (38). Therefore, we injected WT and *Mr1*$^{-/-}$ mice with a low (25 μg) or high dose (300 μg) of MCA and monitored their long-term survival (Fig. 1F and G). At a low dose of MCA, *Mr1*$^{-/-}$ mice displayed greater resistance to MCA-induced fibrosarcoma than WT mice, with 5 of 21 *Mr1*$^{-/-}$ mice and 12 of 21 WT mice developing tumors (Fig. 1F and G). Similarly, this resistance was also observed in *Mr1*$^{-/-}$ mice injected with a high dose of MCA compared with WT mice, suggesting that a lack of MAIT cells permitted for better protection against tumor initiation.

To determine how loss of MAIT cells affected tumors growing outside of mucosal sites, we subcutaneously injected SM1WT1 melanoma cells, from which the LWT1 melanoma line was derived, into WT or *Mr1*$^{-/-}$ mice. Again, we observed a significant reduction of SM1WT1 tumor growth in *Mr1*$^{-/-}$ mice compared with WT mice (Fig. 1H). Furthermore, growth suppression was dependent on NK cells, CD8^{+} T cells, and IFNγ, as SM1WT1 tumor–bearing *Mr1*$^{-/-}$ mice depleted or neutralized of this cell type or cytokine, respectively, were unable to suppress tumor growth compared with cIg-treated groups (Fig. 1I–J).

MAIT Cells Promote Experimental Lung Metastases

To further demonstrate that MAIT cells had a tumor-promoting function, we asked whether adoptive transfer of MAIT cells into *Mr1*$^{-/-}$ mice reversed the reduction in lung metastases (Fig. 2A and B). MAIT cells were identified and sorted using MR1 tetramers (Supplementary Fig. S1A). Using the protocol as indicated in the schematic (Fig. 2A), whole splenocytes (containing MAIT and conventional T cells) from WT mice were cultured in the presence of the activating MAIT cell ligand 5-OP-RU and IL2 for 6 to 7 days

Published OnlineFirst December 11, 2019; DOI: 10.1158/2159-8290.CD-19-0569

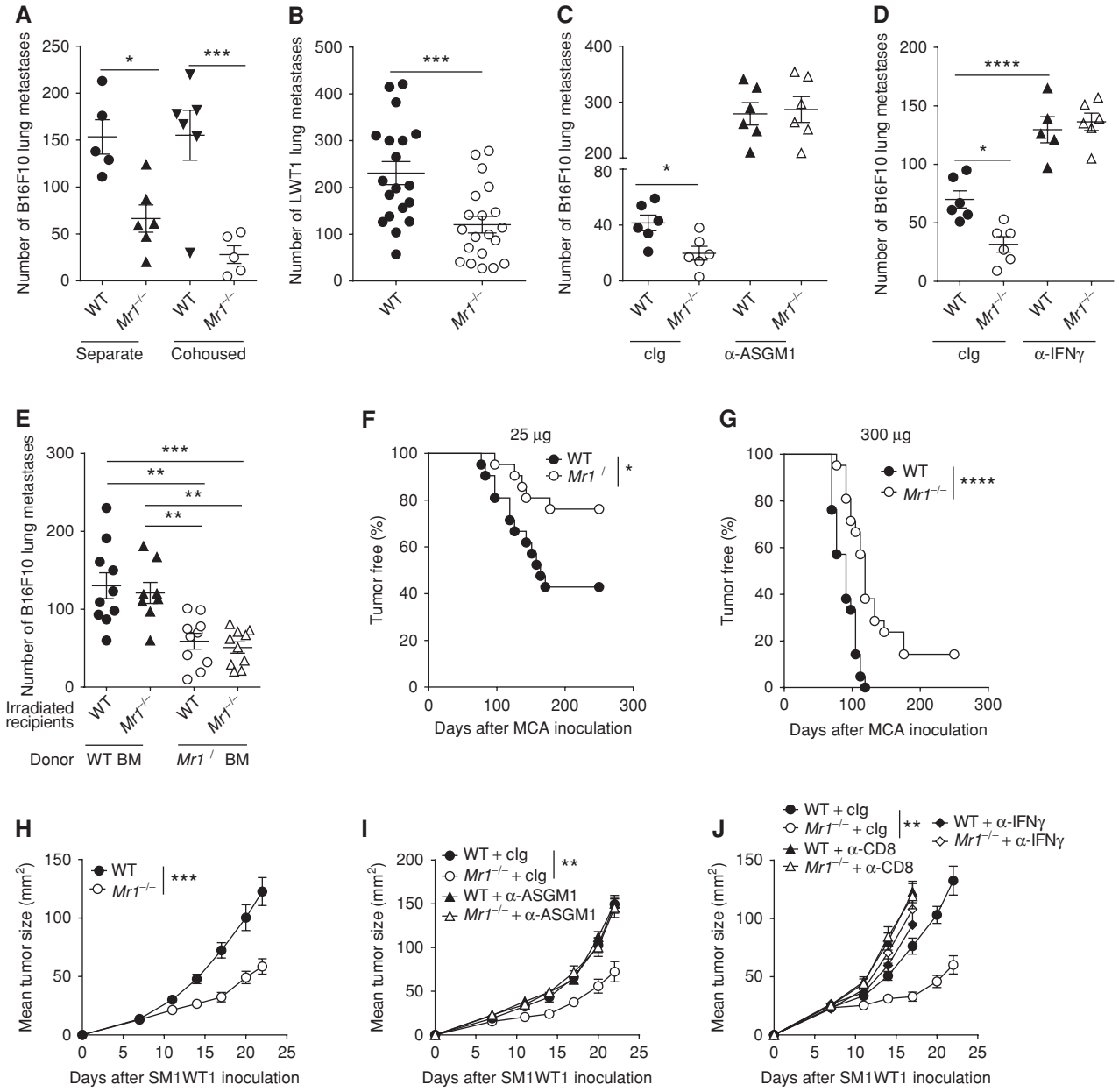

Figure 1. Tumor initiation, growth, and metastases are suppressed in *Mr1*$^{-/-}$ mice. Groups of C57BL/6 WT or *Mr1*$^{-/-}$ mice ($n = 5$–8/group) were injected intravenously with 1×10^5 B16F10 melanoma cells (**A**), 5×10^5 LWT1 melanoma cells (**B**), or 5×10^4 B16F10 melanoma cells (**C** and **D**) on day 0. **E,** Groups of BM chimeric mice ($n = 8$–10/group) were injected intravenously with 1×10^5 B16F10 cells 10 weeks after BM transplantation. In some groups, mice were treated intraperitoneally with cIg or anti-ASGM1 (50 μg/mouse, days −1, 0, and 7; **C**), cIg or anti-IFNγ (750 μg/mouse, day −1; 250 μg/mouse, days 0 and 7; **D**) relative to tumor cell inoculation. On day 14 relative to tumor cell inoculation, lungs were harvested and the metastatic burden was quantified by counting colonies on the lung surface. Data presented as mean ± SEM. Groups of C57BL/6 WT and *Mr1*$^{-/-}$ mice ($n = 21$/group) were injected subcutaneously with MCA at 25 μg (**F**) or 300 μg (**G**). Mice were subsequently monitored for tumor development over 250 days. Kaplan–Meier curves for overall survival of each group are shown. **H–J,** Groups of C57BL/6 WT mice and *Mr1*$^{-/-}$ mice ($n = 6$–8/group) were injected subcutaneously with 1×10^6 SM1WT1 melanoma cells on day 0. In some groups, mice were treated intraperitoneally with either cIg or anti-ASGM1 (50 μg/mouse; **I**), cIg (250 μg/mouse), anti-CD8β (100 μg/mouse), or anti-IFNγ (250 μg/mouse; **J**) on days −1, 0, 7, and 14, relative to tumor cell inoculation. Mice were monitored for tumor growth (calculated by the product of two perpendicular axes). The data show the mean tumor size (mm^2) ± SEM. In **A,** the experiment was performed using WT and *Mr1*$^{-/-}$ mice that were cohoused in the same cages or separate cages whereas in **B–J**, WT and *Mr1*$^{-/-}$ mice were all cohoused. Experiments were performed twice for **A, C, D, I,** and **J**, whereas **B** is pooled from three independent experiments. All other experiments were performed once. Significant differences between groups as indicated by crossbars were determined using a one-way ANOVA followed by Tukey *post hoc* test (**A, C–E, I,** and **J**), a Mann–Whitney test (**B** and **H**), or a log-rank (Mantel–Cox) test for **F** and **G**. *, $P < 0.05$; **, $P < 0.01$; ***, $P < 0.001$; ****, $P < 0.0001$.

Published OnlineFirst December 11, 2019; DOI: 10.1158/2159-8290.CD-19-0569

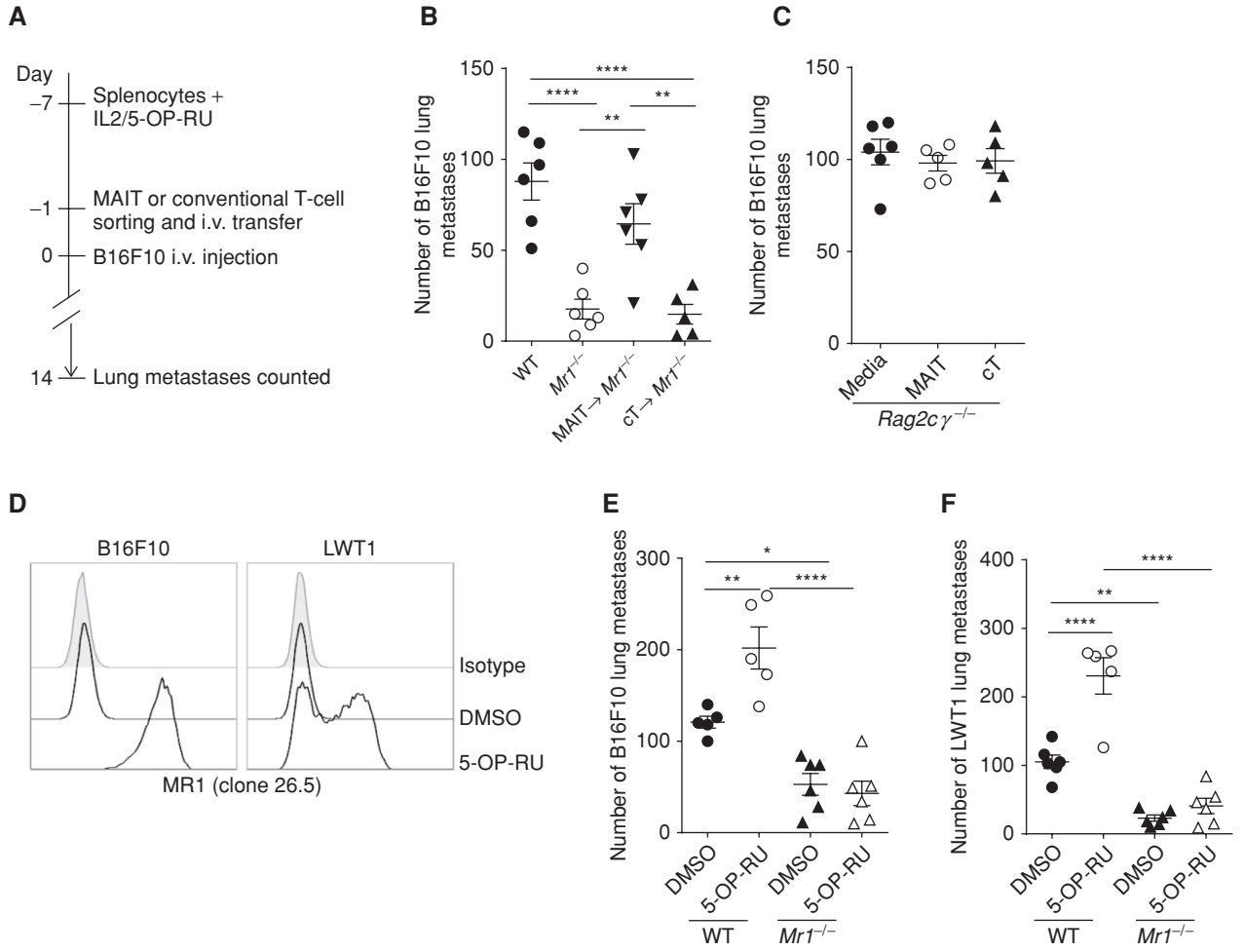

Figure 2. Upregulation of MR1 on B16F10 cells increases lung metastases in a MAIT cell–dependent manner. **A,** The schematic and timeline of MAIT cell expansion from splenocytes derived from C57BL/6 WT mice with IL2 and 5-OP-RU, for sorting and adoptive transfer into tumor-bearing mice. Groups of WT or *Mr1*$^{-/-}$ or *Rag2cγ*$^{-/-}$ mice ($n = 5$–6/group) were injected intravenously (i.v.) with 1×10^5 (**B**) or 1×10^4 (**C**) B16F10 melanoma cells. In some groups, sorted MAIT or conventional T cells ($_c$T; non-MAIT αβ$^+$ T cells; 2×10^5 cells/mouse) from C57BL/6 WT (**B**) or *Tcrd*$^{-/-}$ (**C**) mice were intravenously injected into the indicated groups of mice 1 day before tumor inoculation. **C,** One group of mice received intravenous injection of media alone as a control. **B** and **C,** On day 14 relative to tumor cell inoculation, lungs were harvested, and the metastatic burden was quantified by counting colonies on the lung surface. Data presented as mean ± SEM. **D,** B16F10 or LWT1 melanoma cells were stimulated *in vitro* with DMSO or 5-OP-RU (100 nmol/L) for 4 hours before cell-surface MR1 expression was determined by flow cytometry. Groups of C57BL/6 WT or *Mr1*$^{-/-}$ mice ($n = 5$–6/group) were intravenously injected with 1×10^5 B16F10 (**E**) or 5×10^5 LWT1 (**F**) melanoma cells pulsed with DMSO or 5-OP-RU (100 nmol/L, 4 hours). Fourteen days later, relative to tumor cell inoculation, lungs were harvested, and the metastatic burden was quantified by counting colonies on the lung surface. Data presented as mean ± SEM. Experiments performed twice for **B** and **C,** three times for **D** and **E,** with one representative experiment shown, and once for **F**. Significant differences between groups as indicated by crossbars were determined using a one-way ANOVA followed by Tukey *post hoc* test (**B, E,** and **F**). *, $P < 0.05$; **, $P < 0.01$; ****, $P < 0.0001$.

(8, 24). Subsequently, 2×10^5 MAIT cells (sorted on MR1–5-OP-RU tetramer) or the remaining *Mr1*–5-OP-RU tetramer-negative T cells (termed cT) were injected into *Mr1*$^{-/-}$ mice 1 day before B16F10 intravenous injection (Fig. 2B). Although *Mr1*$^{-/-}$ mice have decreased lung metastases compared with WT mice, this phenotype was strikingly lost in *Mr1*$^{-/-}$ mice that received adoptively transferred MAIT cells, and they displayed similar numbers of lung metastases as WT mice (Fig. 2B). In contrast, transfer of cT cells into *Mr1*$^{-/-}$ mice did not reverse the observed reduction in lung metastases (Fig. 2B). Upon metastasis enumeration at day 14, we were still able to detect MAIT cells in the lungs of MAIT→*Mr1*$^{-/-}$ mice (Supplementary Fig. S1B).

We also expanded MAIT cells from *Tcrd*$^{-/-}$ mice, because they have a higher proportion of MAIT cells compared with WT mice (Supplementary Fig. S1C–S1F), and thus logistically it was easier to expand sufficient MAIT cells for subsequent adoptive transfer experiments. To determine if the metastasis-promoting function of MAIT cells was mediated through direct interaction with tumor cells to promote their growth or indirectly through suppression of NK cells, which are the critical effector cells in the control of experimental lung metastases (Fig. 1C; ref. 39), we performed a similar adoptive transfer experiment of MAIT cells or cT cells derived from *Tcrd*$^{-/-}$ mice into *Rag2cγ*$^{-/-}$ mice, which lack T, B, and NK cells. In contrast to *Mr1*$^{-/-}$ mice, adoptive

Published OnlineFirst December 11, 2019; DOI: 10.1158/2159-8290.CD-19-0569

MAIT cell transfer into *Rag2cγ*$^{-/-}$ mice did not further increase B16F10 lung metastases in these mice compared with the control media–injected group (Fig. 2C). Similarly, cT cell transfer did not directly promote or suppress lung metastases. Importantly, we also demonstrated that MAIT cells expanded from *Tcrd*$^{-/-}$ mice reversed the suppression of B16F10 metastases in *Mr1*$^{-/-}$ mice (Supplementary Fig. S1G) similar to WT MAIT cells (Fig. 2B). Overall, our data demonstrated that MAIT cells had metastasis-promoting function.

Upregulation of MR1 on B16F10 Tumor Cells Increases Metastases

In both mouse and human, MR1 mRNA transcripts have been reported to be present in different tissues, immune cells (such as antigen-presenting cells), and cell lines (40), although its expression in human cell lines can be upregulated and stabilized following incubation with the MAIT cell ligands 5-OP-RU or Ac-6-FP (8, 41, 42). However, surface MR1 expression on immune cells has been reported to be extremely difficult to detect by flow cytometry (41, 42), which we confirmed, even when two different clones of anti-MR1 (26.5, 8F2.F9) were used (Supplementary Fig. S2A–S2F). As previously reported, low levels of MR1 were detected intracellularly in double-positive mouse thymocytes (42), but not in other immune cells such as NK cells and T cells. In contrast, whether mouse tumor cell lines expressed surface MR1 has not been examined. Therefore, we first determined the cell-surface expression of MR1 on a panel of 11 different mouse tumor cell lines using the 26.5 clone of anti-MR1, which cross-reacts with both mouse and human MR1 (Fig. 2D; Supplementary Fig. S3A and S3B; ref. 42). Basally, the level of MR1 was almost undetectable on the surfaces of all tumor cell lines examined (Fig. 2D; Supplementary Fig. S3A and S3B). When we incubated these cell lines with 100 nmol/L of the activating MAIT cell ligand 5-OP-RU and assessed for MR1 surface expression 4 hours later, interestingly, we observed MR1 expression was substantially upregulated on the cell surface of B16F10 and LWT1 melanoma cells (Fig. 2D). MR1 expression was also upregulated to a varying extent on MC38-parental or MC38-OVA–expressing colorectal adenocarcinoma cells, HcMel3, HcMel12, and SM1WT1 melanoma cells, and MCA1956 fibrosarcoma cells (Supplementary Fig. S3A). However, MR1 was not upregulated on RM1 prostate carcinoma cells, 4T1.2 mammary carcinoma cells, or 3LL lung carcinoma cells (Supplementary Fig. S3B). We selected the 100 nmol/L concentration and 4-hour timepoint to assess MR1 upregulation because we demonstrated in a separate dose titration and time kinetic experiments using B16F10 that these conditions optimally upregulated surface MR1 on these cells (as little as 10 nmol/L ligand upregulated MR1; Supplementary Fig. S3C and S3D). The kinetics of MR1 upregulation on B16F10 cells was similar to what was previously reported for human C1R cells (B-cell lymphoblastoid cell line; ref. 41). Similarly, MR1 was generally negative or very low across a range of different human tumor cell lines, which became upregulated following incubation with 5-OP-RU (Supplementary Fig. S3E–S3G). Next, we assessed how upregulation of MR1 on B16F10 or LWT1 cells prior to intravenous injection to WT or *Mr1*$^{-/-}$ mice affected the number of lung metastases. Strikingly, we observed a significantly increased number of lung metastases in WT mice injected with 5-OP-RU–treated compared with DMSO control–treated B16F10 cells and LWT1 cells, and this increase was lost when tumor cells were injected into *Mr1*$^{-/-}$ mice (Fig. 2E and F). Interestingly, RM1, which does not upregulate MR1 following incubation with 5-OP-RU, displayed a similar number of metastases when injected into WT or *Mr1*$^{-/-}$ mice (Supplementary Fig. S3H). Overall, these results suggested that mouse tumor cell lines that are capable of expressing surface MR1 and presenting activating ligands activate MAIT cells to mediate their suppressive function. Furthermore, our data also suggest that the tumor MR1–MAIT interaction rather than host MR1–MAIT interaction was important in promoting experimental lung metastases.

MAIT Cells Promote Metastasis by Suppressing NK-Cell Effector Function

We next investigated the consequences of MR1 upregulation on B16F10 on NK-cell effector function (Fig. 3). B16F10 cells were incubated with 5-OP-RU or DMSO vehicle control for 4 hours, before cells were washed and intravenously injected into WT mice. On day 5, the lungs were harvested, and NK-cell effector function, as measured by IFNγ production and degranulation (CD107a), was assessed (Fig. 3A). Strikingly, the proportion of NK cells producing IFNγ and their expression levels as measured by mean florescence intensity (MFI) were significantly decreased in the lungs of mice bearing 5-OP-RU–treated compared with DMSO-treated B16F10 cells (Fig. 3B and C). In contrast, NK-cell function was not suppressed in the lungs of *Mr1*$^{-/-}$ mice challenged with 5-OP-RU–treated B16F10 cells compared with DMSO-treated B16F10 cells (Fig. 3B and C). Similarly, the proportions of NK cells expressing CD107a and their expression levels were also significantly decreased in the lungs of mice injected with 5-OP-RU–treated B16F10 cells compared with DMSO-treated B16F10 cells (Fig. 3D and E). We observed a similar suppression of NK-cell effector function when the lungs of mice injected with B16F10 cells treated with two different doses of 5-OP-RU were harvested and analyzed at a later time point on day 11 (Supplementary Fig. S4A–S4E). In WT mice that received 5-OP-RU–treated LWT1, we again observed suppression of NK-cell effector function but this did not manifest in *Mr1*$^{-/-}$ mice (Fig. 3F–I). Interestingly, we also observed an increased proportion of NK cells producing IFNγ derived from the lungs of *Mr1*$^{-/-}$ mice injected with DMSO-treated LWT1 compared with similarly injected WT mice. Overall, these data demonstrated that the interaction of MAIT cells with MR1-expressing B16F10 or LWT1 tumor cells played a critical role in suppressing the antimetastatic activity of NK cells.

Increased Production of IL17A and TNF in MAIT Cells Derived from the Lungs of Mice Injected with 5-OP-RU–Treated B16F10 Cells

Given that MAIT cells can rapidly secrete effector cytokines, we therefore determined whether their activation status and cytokine profile were modulated in the lungs of mice injected

Published OnlineFirst December 11, 2019; DOI: 10.1158/2159-8290.CD-19-0569

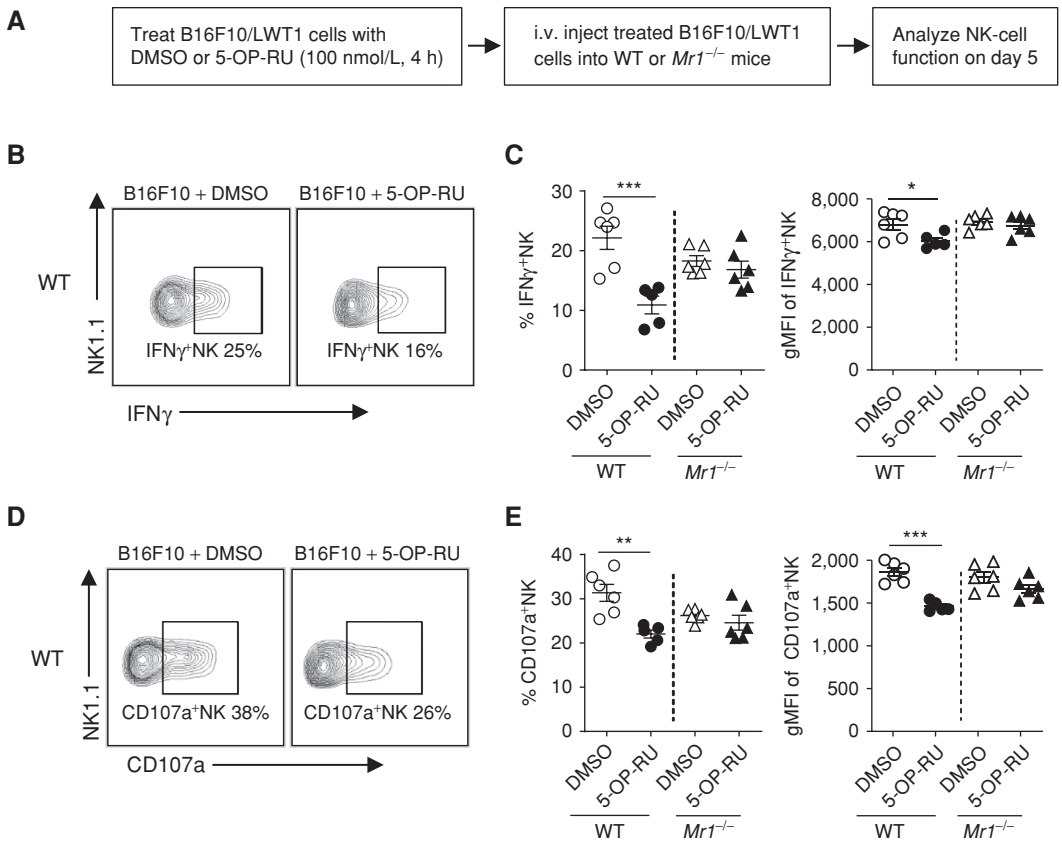

Figure 3. Tumor upregulation of MR1 suppresses NK-cell function via MAIT cells. **A,** Schematic to analyze NK effector function in the lungs of C57BL/6 WT or *Mr1*$^{-/-}$ mice injected with 5-OP-RU–pulsed B16F10 or LWT1 cells. On day 5 relative to tumor inoculation, single-cell suspensions from lungs from the indicated groups of mice ($n = 5$–6/group) were stimulated with PMA/ionomycin plus protein transport inhibitors for 3 hours, and NK-cell effector function was assessed by flow cytometry. **B,** Representative contour plots of IFNγ staining in NK cells (NKp46$^+$NK1.1$^+$TCRβ$^-$ CD45.2$^+$) and the (**C**) proportion and geometric MFI (gMFI) of IFNγ$^+$ NK cells among total NK cells in B16F10-bearing lungs. **D,** Representative contour plots of CD107a staining in NK cells and (**E**) the proportion and geometric MFI of CD107a$^+$ NK cells among total NK cells in B16F10 tumor–bearing lungs. (*continued on following page*)

with 5-OP-RU– or DMSO-treated B16F10 cells (Fig. 4A). CD69 is a commonly used marker to determine MAIT cell activation status and tissue residency (23), and we observed an increased proportion of MAIT cells that expressed CD69, IL17A, and TNF in the lungs of mice injected with 5-OP-RU–treated compared with DMSO-treated B16F10 tumor cells following restimulation with PMA/ionomycin (Fig. 4B–F). Interestingly, the proportion of MAIT cells producing IFNγ did not change (Fig. 4G). In contrast, *in vitro* coculture of purified splenic MAIT cells expanded using the same condition as described for Fig. 2 with 5-OP-RU–treated compared with DMSO-treated B16F10 cells produced more IFNγ, IL17A, and TNF (Supplementary Fig. S5A–S5C). This response was specific as no increase in cytokine production was observed in conventional T cells cultured with 5-OP-RU–treated compared with DMSO-treated B16F10 (Supplementary Fig. S5D–S5F). Similar to previous reports that human MAIT cells displayed cytotoxic capability (30, 31, 34), we observed a decrease in the number of 5-OP-RU–treated Cell Trace Violet–labeled B16F10 cells following coculture with MAIT cells (Supplementary Fig. S5G) but not with conventional T cells (Supplementary Fig. S5H). These data suggested that the antitumor phenotype of MAIT cells observed *in vitro* may not reflect their physiologic role *in vivo*.

Given the increased proportion of IL17-producing MAIT cells, we asked how the loss of IL17A affected NK-cell effector function. WT or *Il17a*$^{-/-}$ mice were injected with 5-OP-RU– or DMSO-treated B16F10 cells, and 5 days later the lungs were harvested for NK-cell analysis. Although the proportions of IFNγ-producing and CD107a-expressing NK cells were significantly reduced in WT mice, as demonstrated earlier, we did not observe this reduction in *Il17a*$^{-/-}$ mice (Fig. 4H and I), suggesting that IL17A may be one mechanism by which the antimetastatic activity of NK cells is suppressed. To confirm IL17A was derived from MAIT cells, we adoptively transferred MAIT cells from WT or *Il17a*$^{-/-}$ mice into *Mr1*$^{-/-}$ mice bearing B16F10 lung metastases (Fig. 4J). MAIT cells that were unable to produce IL17A were significantly less effective at reversing the suppressive phenotype compared with WT MAIT cells, demonstrating that IL17A was partially required for suppression. By inference, there must be additional MAIT cell mechanisms because full reversal of metastasis suppression was not achieved by *Il17a*$^{-/-}$ MAIT cells.

Published OnlineFirst December 11, 2019; DOI: 10.1158/2159-8290.CD-19-0569

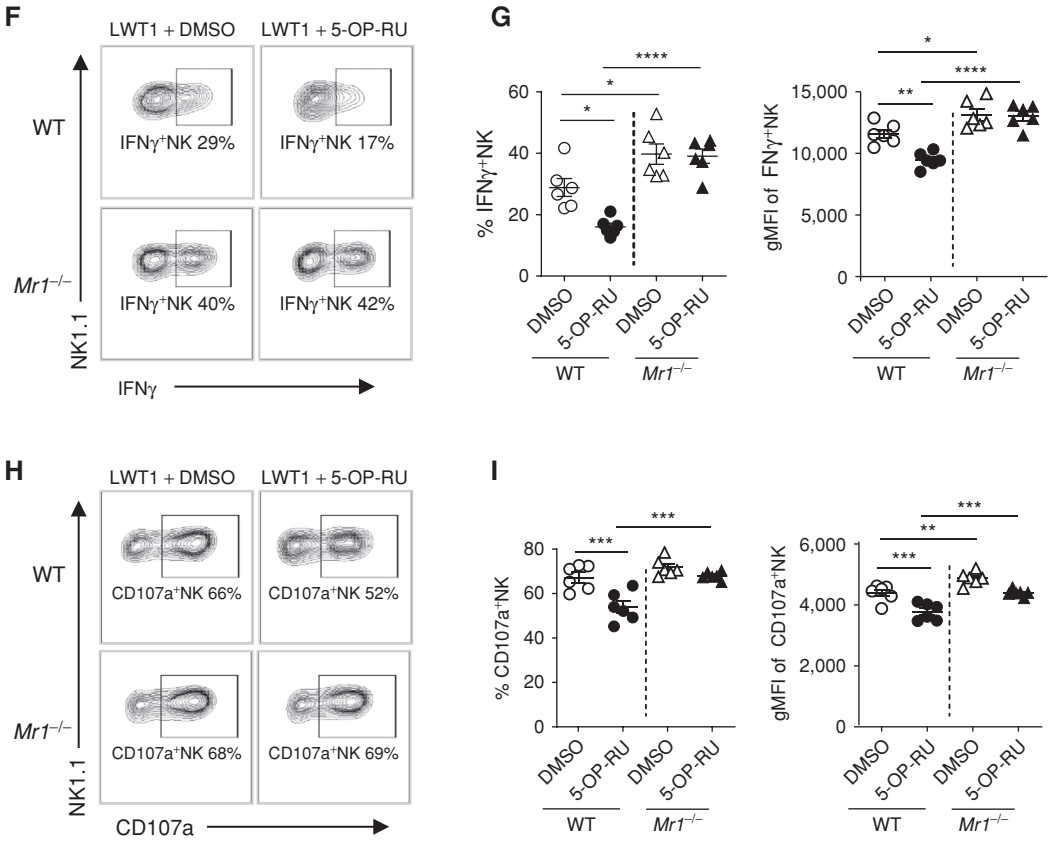

Figure 3. ***(Continued)*** **F,** Representative contour plots of IFNγ staining in NK cells and (**G**) the proportion and geometric MFI of IFNγ+ NK cells among total NK cells in LWT1 tumor–bearing lungs. **H,** Representative contour plots of CD107a staining in NK cells and (**I**) the proportion and geometric MFI of CD107a+ NK cells among total NK cells in LWT1-bearing lungs. Data presented as mean ± SEM. Experiments performed once for **B–E** and twice for **F–I**. Significant differences between groups as indicated by crossbars were determined using a one-way ANOVA followed by Tukey *post hoc* test. *, $P < 0.05$; **, $P < 0.01$; ***, $P < 0.001$; ****, $P < 0.0001$. i.v., intravenous.

Loss of Surface MR1 on B16F10 Cells Decreases Their Metastatic Potential in WT Mice

Our data suggested the importance of MR1 expression on B16F10 cells to activate the suppressive function of MAIT cells. Using CRIPSR/Cas9, three different single-guide RNAs (sgRNA) targeting the mouse MR1 gene were designed and transfected into B16F10 cells, respectively, whereas transfection of B16F10 cells with an empty vector served as a control (Fig. 5). As shown in Fig. 5A, all three sgRNAs effectively knocked out MR1 in B16F10 cells (B16F10-MR1^{KO}) compared with vector control–transfected B16F10 tumor cells. Using *in vitro* assays, we confirmed that loss of MR1 in B16F10 cells did not intrinsically affect their biology, as we observed no changes in their proliferation or migration ability (Supplementary Fig. S6A–S6B). Similarly, coculture of B16F10 cells with 5-OP-RU did not alter the biology of these cells as measured by their proliferative or migratory assays (Supplementary Fig. S6C–S6D). Next, we intravenously injected the three B16F10-MR1^{KO} or vector control B16F10 tumor cell lines into WT and *Mr1*$^{-/-}$ mice and determined their lung metastasis burden 14 days later (Fig. 5B). Strikingly, the number of metastases was dramatically reduced in WT mice injected with the B16F10-MR1^{KO} cell lines compared with those that received vector control B16F10 (Fig. 5B). Furthermore, for all three B16F10-MR1^{KO} cell lines, we observed no further decrease in metastases in the *Mr1*$^{-/-}$ mice compared with WT mice (Fig. 5B). We demonstrated this decrease in metastases was due to the loss of MR1 and not caused by the transfection process, as the number of metastases was similar in WT mice injected with parental or vector control B16F10 (Supplementary Fig. S6E). *In vivo*, we also confirmed that the loss of MR1 on B16F10 cells did not intrinsically affect their ability to form lung metastases, as similar numbers were observed between *Rag2cγ*$^{-/-}$ mice intravenously injected with B16F10 vector control or B16F10-MR1^{KO} (sgR3) (Fig. 5C).

When we overexpressed MR1 in B16F10-MR1^{KO} (sgR3) cells, we showed we could again upregulate MR1 on the cell surface following coculture with 5-OP-RU (Fig. 5D). Interestingly, injection of B16F10 overexpressing MR1 into WT mice increased the number of metastases compared with the GFP vector control–transfected B16F10-MR1^{KO} (sgR3) cell line even in the absence of pretreatment with 5-OP-RU (Fig. 5E). One possibility is that MR1 overexpression may directly suppress NK-cell function given its similarity to MHC I. However, this is unlikely given that the number of metastases in *Mr1*$^{-/-}$ mice injected with B16F10 or B16F10-MR1^{KO} was similar (Fig. 5B). Another possibility is that the increased availability

Published OnlineFirst December 11, 2019; DOI: 10.1158/2159-8290.CD-19-0569

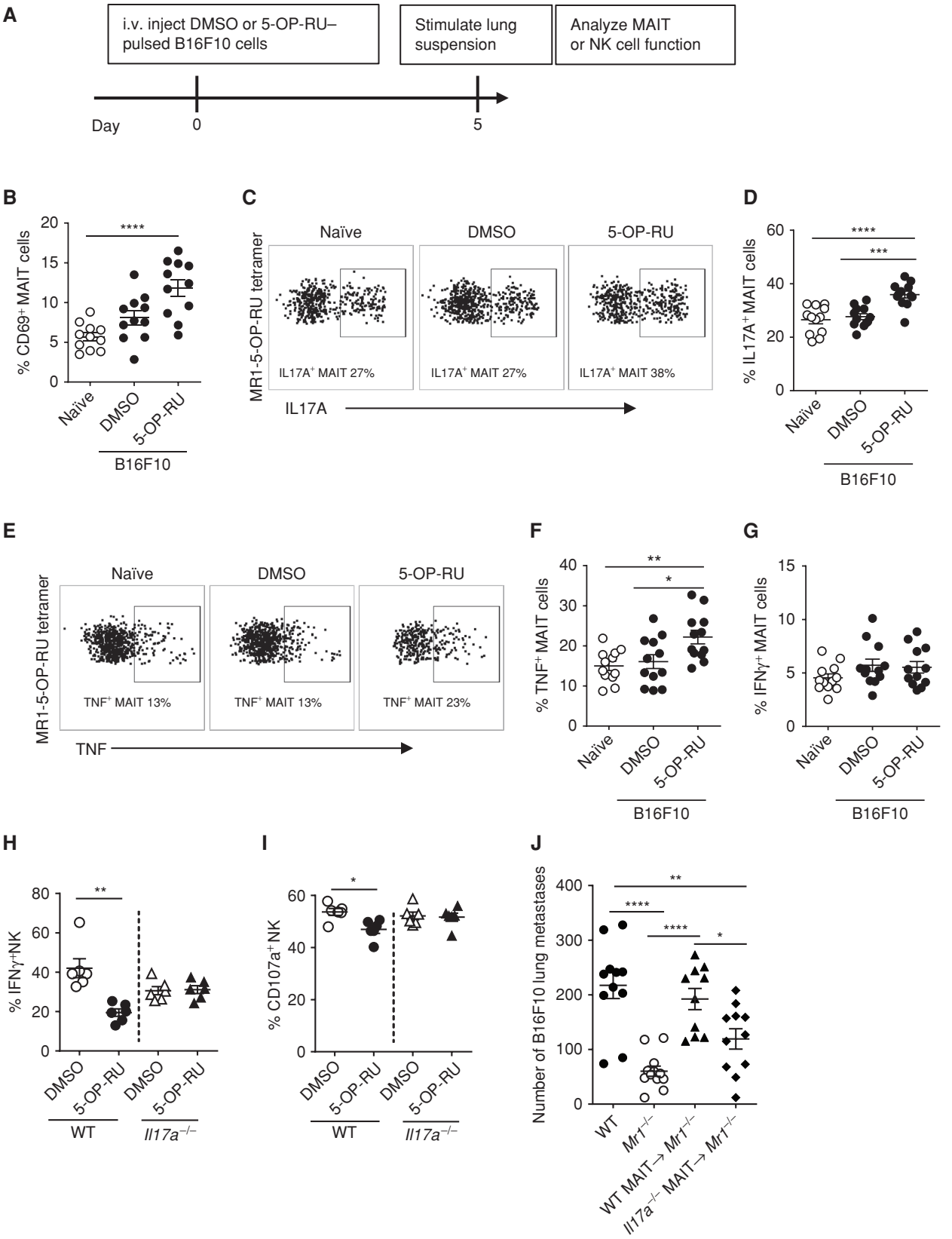

Published OnlineFirst December 11, 2019; DOI: 10.1158/2159-8290.CD-19-0569

of MR1 allows more efficient loading of endogenous stimulatory MAIT ligands, which consequently activates more MAIT cells. Some MR1 binding ligands such as 5-OP-RU upregulate and activate MAIT cells, whereas other ligands such as Ac-6-FP upregulate MR1 (Supplementary Fig. S6F) and inhibit MAIT cells (10, 11). To determine whether activation of MAIT cells was required for their suppression of NK cells, Ac-6-FP– or vehicle-treated B16F10 cells were injected into WT or *Mr1*$^{-/-}$ mice (Fig. 5F). Strikingly, we observed a decrease in the number of metastases in WT mice injected with Ac-6-FP–treated compared with vehicle-treated B16F10 tumor cells. This level of reduction in metastases was similar to *Mr1*$^{-/-}$ mice injected with Ac-6-FP–treated or vehicle-treated B16F10 cells (Fig. 5F). Intriguingly, these data suggested that endogenous MAIT ligands derived from either the microbiota, tumors, and/or the TME activated MAIT cells that can be blocked with an inhibitory MAIT ligand. Overall, our data indicated the potential for tumors to upregulate MR1 and activate MAIT cell immunoregulatory function.

Blockade of MR1 Suppresses Experimental Lung Metastases and Subcutaneous Tumor Growth

In addition to their use in flow-cytometry analysis, the 26.5 and 8F2.F9 clones of anti-MR1 block MAIT cells from interacting with MR1 (42, 43). Therefore, we asked whether the effect we observed in *Mr1*$^{-/-}$ mice was recapitulated with these MR1-blocking antibodies (Fig. 6). MR1 blockade by clone 26.5 on days −1, 0, 3, and 7, relative to B16F10 intravenous injection, effectively suppressed lung metastases to a similar level as observed in *Mr1*$^{-/-}$ mice (Fig. 6A). Furthermore, we confirmed the specificity of 26.5, as no further decrease in the number of lung metastases was observed between tumor-bearing *Mr1*$^{-/-}$ mice treated with 26.5 or cIg (Fig. 6A). Next, we compared whether giving three or four doses of clone 26.5 or 8F2.F9 (days −1, 0, 3 vs. days −1, 0, 3, and 7) equivalently suppressed metastases (Fig. 6B). Interestingly, suppression of lung metastases was more effective when four doses of 26.5 were given compared with three doses (Fig. 6B). In contrast, administering three or four doses of 8F2.F9 equivalently reduced B16F10 lung metastases, and this suppression appeared to be superior to that observed using the 26.5 clone (Fig. 6B). We also confirmed the specificity of the 8F2.F9 clone for MR1, as no further decrease in the number of lung metastases was observed between tumor-bearing *Mr1*$^{-/-}$ mice treated with 8F2.F9 or cIg (Fig. 6B). The lack of any further decrease in lung metastases in *Mr1*$^{-/-}$ mice treated with 26.5 or 8F2.F9 also suggested that these antibodies probably do not directly affect B16F10 metastasis (Fig. 6A and B). Furthermore, we again demonstrated the importance of blocking MR1 on tumors, because the numbers of B16F10-MR1^{KO} (sgR3) lung metastases were not reduced between 8F2.F9- and cIg-treated mice compared with similar groups of treated mice bearing B16F10 parental metastases (Fig. 6C). In addition, we showed that 8F2.F9 treatment significantly reduced the numbers of LWT1 lung metastases compared with cIg treatment (Fig. 6D).

In mice bearing established subcutaneous MCA1956 or SM1WT1 tumors (Fig. 6E and F), treatment with four doses of anti-MR1 significantly suppressed tumor growth compared with cIg-treated groups. Finally, we assessed the therapeutic potential of anti-MR1 therapy in the treatment of established *de novo* MCA-induced fibrosarcomas (Fig. 6G–I). Although cIg-treated fibrosarcomas grew rapidly and all mice succumbed to their tumors (Fig. 6G), anti-MR1 reduced the growth of most tumors (Fig. 6H and I) and caused the complete rejection of 3 of 21 tumors (Fig. 6G). The therapeutic efficacy of anti-MR1 as a monotherapy was impressive compared with historical single immunotherapies that have been evaluated in this exact same model, including anti–PD-1 (44).

Anti-MR1 Therapy Improves Immune Cell Infiltration and Effector Function in Tumors

The therapeutic efficacy of anti-MR1 in suppressing the growth of subcutaneous SM1WT1 tumors (Fig. 6F) suggested that MAIT cells may be present in these tumors. One day after the second treatment with anti-MR1 or cIg, MAIT cells were detected in the tumor-infiltrating lymphocytes (TIL) of SM1WT1 tumors, but their proportion was low among all T cells (Fig. 7A and B). Similar proportions of MAIT cells were observed in TILs regardless of cIg or anti-MR1 treatment. Using flow cytometry, we also assessed TILs from end-stage SM1WT1 tumors derived from mice in Fig. 6F. Interestingly, we observed a significant increase in the proportion of total CD45.2$^+$ immune cells (Fig. 7C), CD8$^+$ T cells (Fig. 7D), and NK cells (Fig. 7E) in the anti-MR1–treated compared with cIg-treated groups. Furthermore, we observed an increased proportion of IFNγ-producing and CD107a-expressing CD8$^+$ T cells and NK cells from the TILs of anti-MR1–treated compared with cIg-treated mice following restimulation with PMA/ionomycin (Fig. 7F–I). Overall, these data suggested

Figure 4. Upregulation of tumor MR1 activates MAIT cells to suppress NK-cell effector function in an IL17-dependent manner. **A,** Schematic describing analysis of MAIT or NK-cell effector function in the lungs of C57BL/6 WT or *Il17a*$^{-/-}$ mice injected with 5-OP-RU– or DMSO-stimulated B16F10 melanoma cells. On day 5 relative to tumor inoculation, single-cell suspensions from lungs were stimulated with PMA/ionomycin plus protein transport inhibitors for 4 hours, and MAIT or NK-cell function was assessed by flow cytometry i.v., intravenous. **B,** The proportions of CD69$^+$ MAIT cells among total MAIT cells (B220$^-$ F4/80$^-$ MR1–5-OP-RU tetramer$^+$ TCRβ$^+$) in naïve or tumor-bearing lungs. Data presented as mean ± SEM. **C,** Representative concatenated dot plots of IL17A expression by MAIT cells. **D,** The proportions of *IL17*$^+$ MAIT cells among total MAIT cells in the lungs of naïve and tumor-bearing mice as indicated. Data presented as mean ± SEM. **E,** Representative concatenated dot plot of TNF expression by MAIT cells. **F,** The proportion of TNF$^+$ MAIT cells and (**G**) IFNγ$^+$ MAIT cells among total MAIT cells in the lungs of naïve and tumor-bearing mice as indicated. **H** and **I,** On day 5 relative to tumor inoculation, lungs were harvested ($n = 6$/group) and stimulated with PMA/ionomycin plus protein transport inhibitors for 3 hours, and NK-cell function was assessed by flow cytometry. The proportion of IFNγ$^+$ NK cells and CD107a$^+$ NK cells among total NK cells (NKp46$^+$ NK1.1$^+$ TCRβ$^-$ CD45.2$^+$) in tumor-bearing C57BL/6 WT or *Il17a*$^{-/-}$ mice is indicated. Data presented as mean ± SEM. **J,** Groups of WT or *Mr1*$^{-/-}$ mice ($n = 4$–6/group) were injected intravenously with 1×10^5 B16F10 melanoma cells. In some groups, sorted MAIT cells (2×10^5 cells/mouse) from C57BL/6 WT or *Il17a*$^{-/-}$ mice were intravenously injected into the indicated groups of mice 1 day before tumor inoculation. On day 14 relative to tumor cell inoculation, lungs were harvested, and the metastatic burden was quantified by counting colonies on the lung surface. Data presented as mean ± SEM. Data were pooled from two independent experiments for **B, D, F, G,** and **J**. Experiments were performed twice for **H** and **I**. Significant differences between groups as indicated by crossbars were determined using a one-way ANOVA followed by Tukey *post hoc* test (**B**, **D, F,** and **J**) or a Mann–Whitney test (**H** and **I**). *, $P < 0.05$; **, $P < 0.01$; ***, $P < 0.001$; ****, $P < 0.0001$.

Published OnlineFirst December 11, 2019; DOI: 10.1158/2159-8290.CD-19-0569

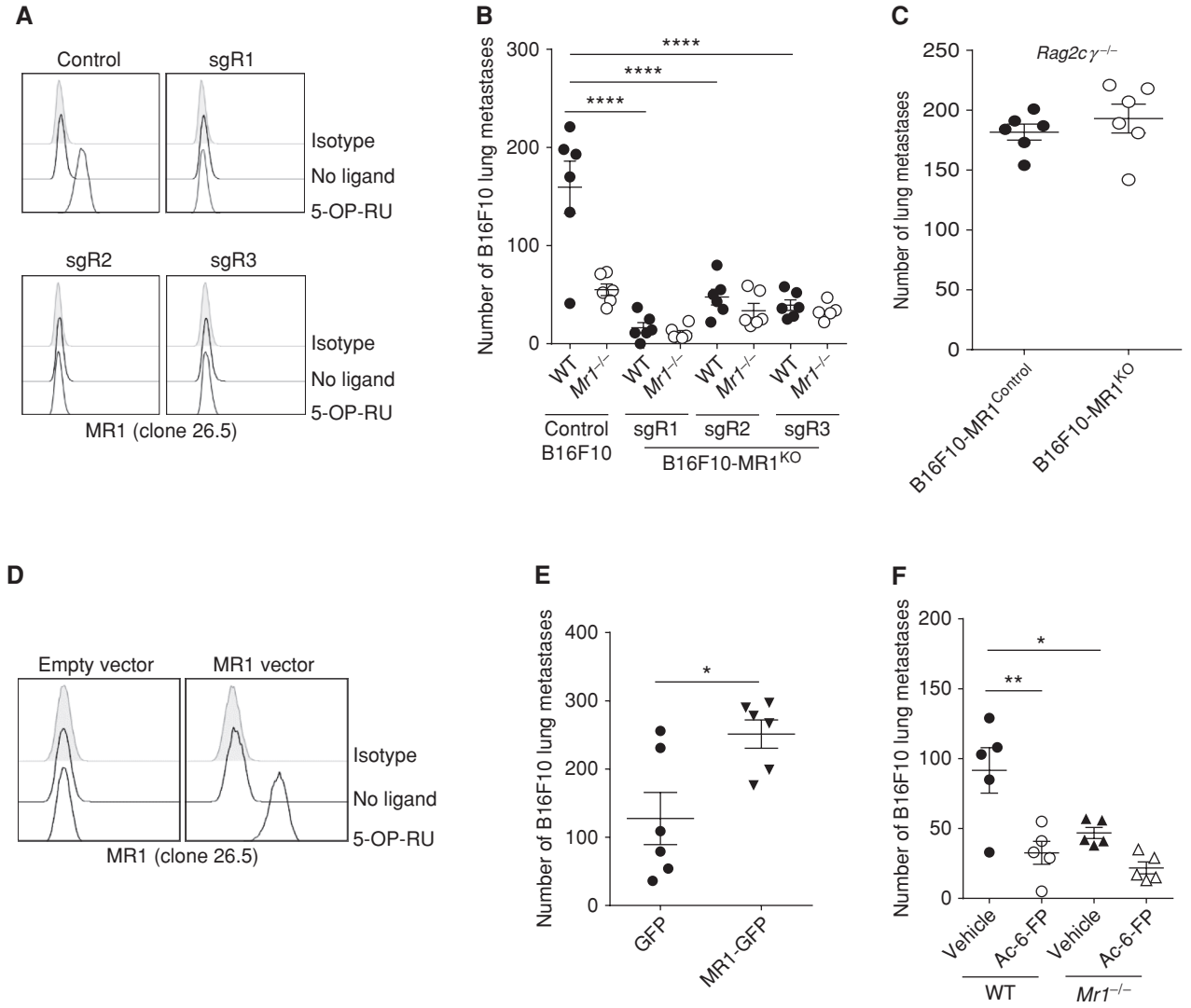

Figure 5. Expression of tumor MR1 is critical for the suppressive function of MAIT cells. **A,** Generation of three independent B16F10 cell lines knocked out for MR1 using three different MR1 sgRNAs. Loss of MR1 surface expression on these cells with or without 5-OP-RU ligand stimulation was verified by flow cytometry. Empty vector–transfected B16F10 cells were used as a positive control. **B** and **C,** Groups of C57BL/6 WT, *Mr1*$^{-/-}$, or *Rag2cγ*$^{-/-}$ mice ($n = 5$–6/group) were intravenously injected with either (**B**) 1×10^5 B16F10 vector control cells or the indicated clone of B16F10 cells lacking MR1 (sgR1, sgR2, and sgR3) or (**C**) 1×10^4 B16F10-MR1^{KO} cells (sgR3 clone). On day 14 relative to tumor cell inoculation, lungs were harvested, and the metastatic burden was quantified by counting colonies on the lung surface. Data presented as mean ± SEM. **D,** Reexpression of GFP- or GFP-MR1–expressing vector into B16F10-MR1^{KO} (sgR3 clone). MR1 surface expression of these cells stimulated with or without 5-OP-RU was assessed by flow cytometry. **E,** Groups of C57BL/6 WT mice ($n = 6$/group) were intravenously injected with 1×10^5 B16F10-MR1^{KO} (sgR3 clone) transfected with empty GFP-expressing vector or MR1-GFP–expressing vector. **F,** Groups of C57BL/6 WT or *Mr1*$^{-/-}$ mice were intravenously injected with parental B16F10 cells treated with vehicle (dd H_2O) or Ac-6-FP (10 μmol/L, 18 hours). On day 14 relative to tumor cell inoculation, lungs were harvested and the metastatic burden was quantified by counting colonies on the lung surface. Data, mean ± SEM. Experiments performed twice for **A–E** and 3 times for **F**. Significant differences between groups as indicated by crossbars were determined by a one-way ANOVA followed by Tukey *post hoc* test (**B** and **F**) or a Mann–Whitney test (**C** and **E**). *, $P < 0.05$; **, $P < 0.01$; ****, $P < 0.0001$.

that the interaction of MR1 on tumors and MAIT cells might be critical in suppressing antitumor immunity in mucosal and nonmucosal sites, and blocking MR1 may represent a new strategy for cancer immunotherapy.

DISCUSSION

In this study, we demonstrated for the first time that MAIT cells promoted tumor initiation, growth, and metastasis. Using two experimental mouse models of lung metastasis, B16F10 and LWT1, a significant decrease in the number of lung metastases was observed in *Mr1*$^{-/-}$ mice compared with WT mice, and this reduction was replicated using two different MR1-blocking antibodies. In addition, *Mr1*$^{-/-}$ mice were more resistant to carcinogen-induced fibrosarcoma development compared with WT mice. Furthermore, we demonstrated, using *Mr1*$^{-/-}$ mice and WT mice treated with anti-MR1, that loss of MAIT cells or MAIT cell activation

Published OnlineFirst December 11, 2019; DOI: 10.1158/2159-8290.CD-19-0569

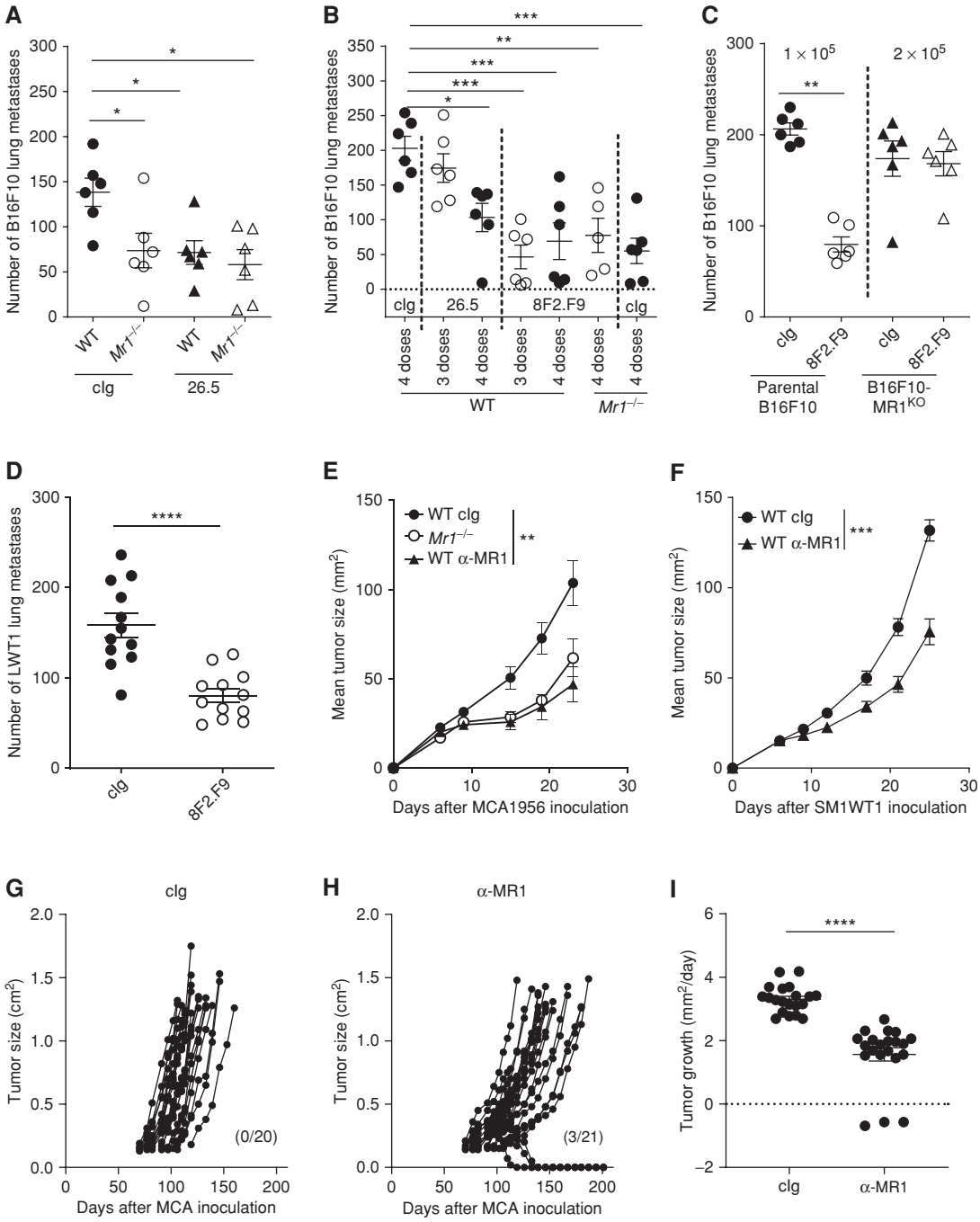

Figure 6. MR1 blockade suppresses experimental lung metastases and subcutaneous tumor growth. Groups of C57BL/6 WT or *Mr1*$^{-/-}$ mice ($n = 5$–6/group) were intravenously injected with 1×10^5 B16F10 (**A** and **B**), 1×10^5 parental B16F10 or 2×10^5 B16F10-MR1^{KO} (sgR3 clone) melanoma cells (**C**), and 5×10^5 LWT1 melanoma cells (**D**) or subcutaneously injected with 1×10^6 MCA1956 fibrosarcoma (**E**) or 1×10^6 SM1WT1 melanoma cells (**F**) on day 0. The indicated groups of mice were intraperitoneally (i.p.) treated with clg or anti-MR1 (clone 25.6 or clone 8F2.F9; 250 μg/mouse) at the indicated doses on days −1, 0, 3, and 7 (**A** and **B**), −1, 0, and 3 (**B**, **C,** and **D**), or 6, 10, 14, and 18 (**E** and **F**), relative to tumor cell inoculation. **A–D,** On day 14, lungs were harvested, and the metastatic burden was quantified by counting colonies on the lung surface. Data presented as mean ± SEM. **E** and **F,** Mice were monitored for tumor growth (calculated by the product of two perpendicular axes). The data show the mean tumor size (mm^2) ± SEM. **G–I,** Groups of C57BL/6 WT mice ($n = 20$–21/group) were injected subcutaneously with 300 μg of MCA. Mice were treated with clg or anti-MR1 (8F2.F9; 250 μg i.p., twice/week) for 6 weeks from the second palpable tumor measurement (0.19–0.38 cm^2, days 77–126 relative to MCA inoculation). Mice were monitored for fibrosarcoma development over 200 days, with measurements made with a caliper square as the product of two perpendicular diameters (cm^2). Data recorded as tumor size in cm^2 of individual mice. **I,** Tumor growth following treatment was also determined by dividing the change in tumor size by the number of days after treatment initiation. Growth rate of each individual mouse is plotted as mean (mm^2/day) ± SEM. All experiments performed once except **C** and **E,** which were performed twice; **D,** which was pooled from two independent experiments; and **F,** which was performed 3 times. Significant differences between groups as indicated by crossbars were determined by a one-way ANOVA followed by Tukey *post hoc* test (**A** and **B**) or a Mann–Whitney test (**C**, **D, E, F,** and **I**). *, $P < 0.05$; **, $P < 0.01$; ***, $P < 0.001$; ****, $P < 0.0001$.

Published OnlineFirst December 11, 2019; DOI: 10.1158/2159-8290.CD-19-0569

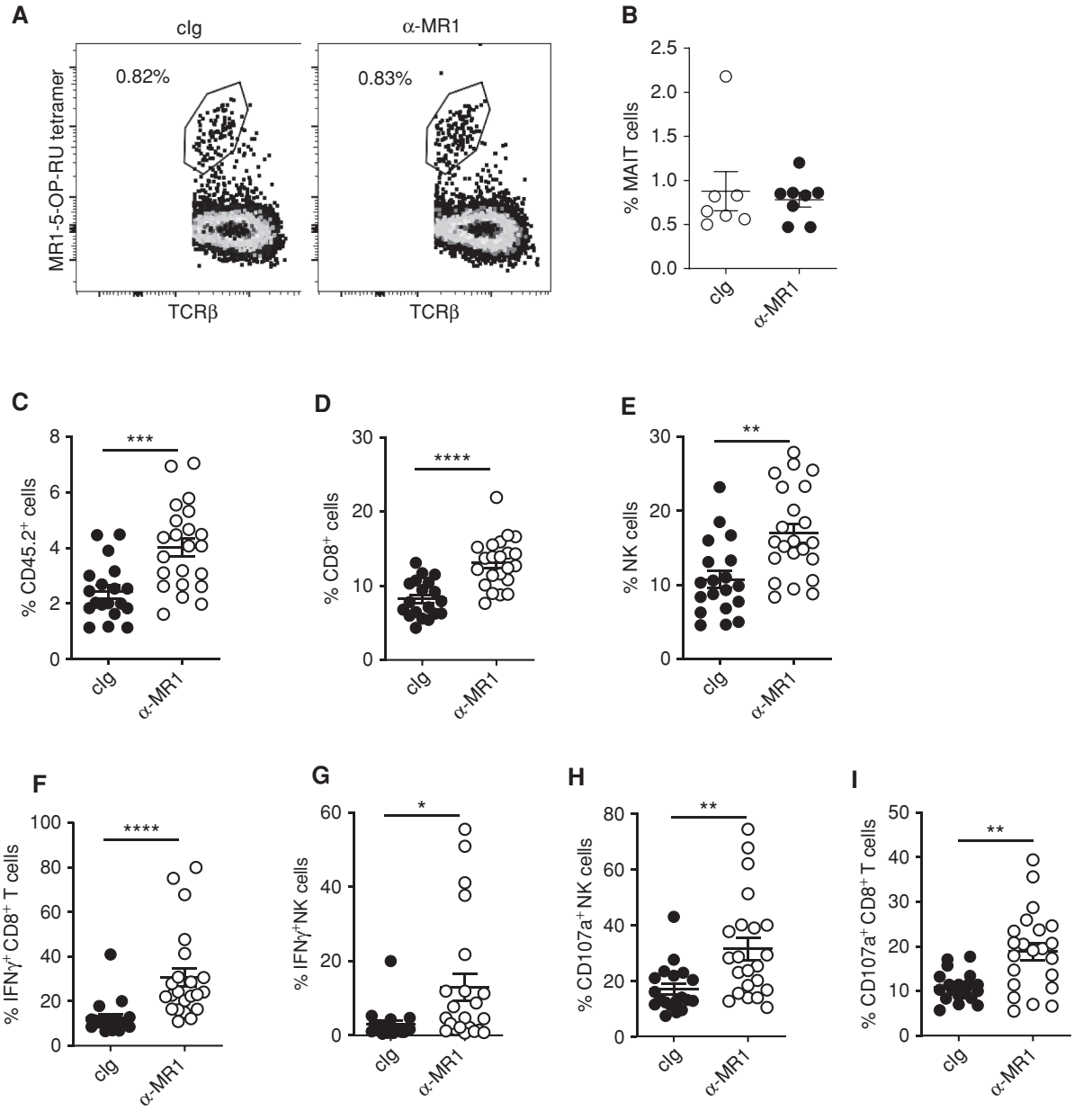

Figure 7. MR1 blockade in SM1WT1 tumors increases immune infiltration and improves effector function. **A** and **B,** Groups of C57BL/6 WT mice ($n = 7$–8/group) were subcutaneously injected with 1×10^6 SM1WT1 melanoma cells on day 0. The mice were intraperitoneally treated with either cIg or anti-MR1 (8F2.F9; 250 μg/mouse) at days 6 and 10 relative to tumor cell inoculation. On day 11, tumors were harvested, and single-cell suspensions were generated for FACS analysis. **A,** Representative dot plots of MAIT cells (5-OP-RU tetramer$^+$ TCRβ$^+$ B220$^-$F4/80$^-$CD45.2$^+$) from the indicated groups. **B,** The proportions of MAIT cells among TCRβ$^+$B220$^-$F4/80$^-$ CD45.2$^+$ cells. Data presented as mean ± SEM. The experiment was performed once. **C–I,** From Fig. 6F and two other independent experiments, end-stage SM1WT1 tumors were harvested (days 23–26), and single-cell suspensions were stimulated with PMA/ionomycin plus protein transport inhibitors for 4 hours prior to FACS analysis. Gating on live CD45.2$^+$ cells, the proportions of (**C**) CD45$^+$ T cells, (**D**) CD8$^+$ T cells (CD8$^+$TCRβ$^+$), (**E**) NK cells (NK1.1$^+$NKp46$^+$TCRβ$^-$), and the proportions of CD8$^+$ T or NK cells that were (**F** and **G**) IFNγ$^+$ or (**H** and **I**) CD107a$^+$ are shown. Data presented as mean ± SEM, and pooled from three independent experiments. Significant differences between groups as indicated by crossbars were determined by a Mann-Whitney test. *, $P < 0.05$; **, $P < 0.01$; ***, $P < 0.001$; ****, $P < 0.0001$.

via MR1, respectively, affected tumors growing outside of mucosal sites such as subcutaneously inoculated MCA1956 and SM1WT1 tumors and *de novo* MCA-induced fibrosarcomas. By performing adoptive transfer of purified MAIT cells into B16F10 tumor–bearing *Mr1*$^{-/-}$ mice, we reversed the reduction in lung metastases in these mice, whereas conventional T-cell transfer was without effect. We also demonstrated that MAIT cells promoted lung metastases by engaging MR1 on tumor cells resulting in an IL17A-dependent suppression of NK-cell effector function. The importance of MR1 expression on tumor cells was further demonstrated by the increased number of metastases in mice injected with 5-OP-RU–pretreated B16F10 tumor cells. In contrast, deletion of MR1 on B16F10 or pretreatment of B16F10 with

Published OnlineFirst December 11, 2019; DOI: 10.1158/2159-8290.CD-19-0569

Ac-6-FP dramatically reduced the number of lung metastases, whereas reexpression of MR1 reversed this phenotype. These data contrasted with previous dogma that MAIT cells were directly cytotoxic to tumor cells, rather illustrating *in vivo* that MAIT cells acted to suppress NK-cell effector function and thereby promote tumor metastasis. This is a new concept in that NK cells are known only to be suppressed by regulatory T cells (45–47), or myeloid/granulocyte populations (48–51), or by MHC class I binding on tumors (52). Here, we have described an important MHC class I–like recognition system that can also affect NK-cell effector function.

In our study, we demonstrated that cell-surface expression of MR1 was highly upregulated in some mouse and human tumor cell lines following incubation with 5-OP-RU in a time- and dose-dependent manner, even when MR1 was undetectable at a basal level. Why certain mouse and human tumor cell lines were unable to upregulate MR1 remains to be investigated. Potential explanations include the absence of a functional WT MR1-encoding gene, or the lack of β2M, which is required for MR1 surface expression (40). Interestingly, the lack of MR1 expression on RM1 tumor cells also corresponded with no decrease in lung metastases in *Mr1*$^{-/-}$ mice compared with WT mice, suggesting the tumor MR1–MAIT interaction was not operating in this TME. It also suggested that host MR1–MAIT interactions were not critical in the RM1 TME. Indeed, the critical importance of MR1 expression on tumors was clearly illustrated when we deleted MR1 in B16F10 cells to generate three different B16F10-MR1^{KO} cell lines. Here, we observed a very striking decrease in B16F10-MR1^{KO} lung metastases compared with similar groups of WT mice injected with control-transfected B16F10 cells. Reexpressing MR1 in B16F10-MR1^{KO} cells increased the number of lung metastases compared with control-transfected cells. This phenotype was not due to an intrinsic effect mediated by MR1 in B16F10 cells, as *in vitro* assays demonstrated these cells displayed similar proliferative and migratory ability as vector control–transfected or parental B16F10 cell lines. Furthermore, injecting B16F10-MR1^{KO} or control-transfected B16F10 cells into *Rag2cγ*$^{-/-}$ mice, which lacked T, B, and NK cells, generated a similar number of lung metastases. This demonstrated the equivalent capability of B16F10-MR1^{KO}– and B16F10-MR1–sufficient cells to form metastases. Finally, we showed that upregulating MR1 on tumor cells increased their metastatic capability. WT mice injected with 5-OP-RU–pulsed B16F10 cells displayed an increased number of lung metastases compared with those that received DMSO-treated B16F10 cells, even when an equal number of both cells were injected. Consequently, NK-cell effector functions including IFNγ production and their degranulation capability were reduced in the lungs of WT mice challenged with 5-OP-RU–treated compared with DMSO-treated B16F10 or LWT1.

Critically, our data also demonstrated that the activation of MAIT cells was required for their suppressive function. Unlike 5-OP-RU, other MAIT cell ligands such as Ac-6-FP and 6-FP, which are derived from vitamin B9, upregulate MR1, but inhibit MAIT cell activation (10, 11). Strikingly, Ac-6-FP–pretreated tumor cells displayed decreased lung metastases compared with vehicle-treated tumor cells, demonstrating that activation of MAIT cells rather than the mere upregulation of MR1 was critical for suppressing antitumor immunity. This also suggested the potential to utilize inhibitory MAIT cell antigen(s) as a therapeutic to suppress MAIT cell activation in tumors. Going forward, a key question is the identification of the source and type of endogenous antigen(s) in mice that activates MAIT cells in the TME. In mucosal sites such as the lungs, the presence of microbial communities containing a complex diversity of bacteria in the lower respiratory tract is now appreciated (53) and can contribute to various pathologies. Using a genetically engineered mouse model of lung cancer, Jin and colleagues demonstrated that the local microbiota associated with tumor growth promoted inflammation and cancer progression via lung-resident γδ T cells (54). We speculate that the presence of tumor cells in the lungs may change the composition of the local microbiome, which may contribute to the release of activating MAIT cell ligands that can upregulate MR1 on tumor cells. Interestingly, a recent study reported that the microbial metabolites in mice controlled the thymic development of MAIT cells (55). Furthermore, the authors demonstrated the ability of 5-OP-RU to rapidly travel from mucosal surfaces to the thymus, where it was captured by MR1 (55). Going forward, it will be important to define the nature of the activating MAIT cell ligands and investigate whether they derived from tumors themselves, the local or gut microbiota, or the TME.

We showed that MAIT cells did not directly promote tumor metastasis, as adoptive transfer of MAIT cells did not increase B16F10 lung metastases in *Rag2cγ*$^{-/-}$ mice that lacked T, B, and NK cells. In *ex vivo* cytokine analysis of MAIT cells derived from the lungs of mice injected with 5-OP-RU–treated B16F10 cells, the proportion of MAIT cells that produced IL17A and TNF, but not IFNγ, increased. We further showed that adoptive transfer of MAIT cells that were unable to produce IL17A into tumor-bearing *Mr1*$^{-/-}$ mice partially reversed the suppressive phenotype. This suggested that IL17A derived from MAIT cells was partially involved in suppressing the antimetastatic activity of NK cells, although clearly other molecules are also involved. Adoptive transfer experiments of MAIT cells deficient in different cytokines could be performed to identify which other cytokines in addition to IL17A are involved in suppressing NK-cell antimetastatic function. Overall, our results clearly demonstrated that tumor cells that express and upregulate MR1 with activating ligands do activate MAIT cell suppression of NK-cell antimetastatic activity.

Despite the difficulty in detecting surface MR1 expression on normal cells by flow cytometry, MR1 was previously reported to be expressed on various immune and epithelial cells as inferred from functional assays using MR1-blocking antibodies (41, 42). Thus, it was possible that MAIT cells could be activated by MR1 expressed on both hematopoietic and nonhematopoietic cells. However, the similar number of lung metastases observed in WT→WT and WT→ *Mr1*$^{-/-}$ chimeric mice implied that MR1 expression on nonhematopoietic cells was not important for MAIT cell development and activation in a tumor setting. Furthermore, given that the numbers of B16F10-MR1^{KO} lung metastases were the same between WT and *Mr1*$^{-/-}$ mice, this suggests any role of MR1 on host immune and nonimmune cells in activating MAIT cells might be comparatively minor. Our data also suggested that the ability of MAIT cells to suppress NK and/or CD8^{+} T cells may not require MR1 on these cell types, given that they did not

Published OnlineFirst December 11, 2019; DOI: 10.1158/2159-8290.CD-19-0569

appear to express surface MR1 and MAIT cell suppression still occurred in *Mr1*$^{-/-}$ mice, where NK cells and CD8$^+$ T cells lacked MR1. Potentially, MAIT ligands can be administered intranasally into tumor-bearing mice to assess which immune cells, if any, in addition to tumor cells, upregulate surface MR1. In humans, basal MR1 expression was generally low or undetectable on many of the tumor cell lines we examined, but was upregulated following culture with 5-OP-RU. Going forward, MR1 protein expression on different tumors and tumor-infiltrating immune cells needs to be characterized and correlated with progression-free survival and overall survival in patients with cancer in general and in those receiving immunotherapy. As most human MAIT cells are CD8 single-positive (18, 25), they potentially may be erroneously identified as conventional CD8$^+$ T cells, and therefore it may be necessary to perform multiplex IHC to determine the presence of MR1, MAIT cells, and CD8 and NK cells in tumors.

Therapeutically, two different clones of MR1 blocking antibodies (26.5 and 8F2.F9) were as capable of reducing B16F10 and LWT1 lung metastases as loss of MAIT cells in *Mr1*$^{-/-}$ mice. Other experiments suggested that their anti-metastatic effect was probably mediated through blocking MAIT cell activation rather than having a direct antitumor effect on MR1-expressing tumor cells. Anti-MR1 alone also suppressed subcutaneous tumor growth of two transplanted tumor cell lines, MCA1956 and SM1WT1, and established *de novo* MCA-induced fibrosarcomas, suggesting that the MR1–MAIT pathway operates in tumors growing in mucosal or nonmucosal sites. SM1WT1 generally does not respond to PD-1 blockade. When we collected end-stage SM1WT1 tumors for flow-cytometry analysis, we observed a significant increase in the proportion of CD8$^+$ T and NK cells in the TILs from anti-MR1–treated groups compared with cIg-treated groups. Furthermore, an increased proportion of these CD8$^+$ T and NK cells displayed improved effector function as observed by expression of IFNγ and CD107a. Given that MR1 is highly conserved across 150 million years of mammalian evolution, blockade of the tumor MR1–MAIT cell axis in humans may represent a novel approach to relieve immune-mediated suppression of NK and CD8$^+$ T cells in the TME. Future experiments and combination approaches can now be used to try to boost NK-cell and CD8$^+$ T-cell antitumor activity by blocking tumor MR1 in tumors where MR1 is highly expressed. For example, blocking MR1 on these tumors might allow better retention of NK/CD8$^+$ T cells and their effector functions in the context of immune-checkpoint blockade or other approaches that reduce myeloid-mediated immunosuppression. Overall, our data provide evidence that MAIT cells suppress NK-cell antimetastatic function and that blocking MR1 or saturating it with an inhibitory ligand may represent a new therapeutic strategy for cancer immunotherapy.

METHODS

Mice

C57BL/6 WT and gene-targeted mice were bred in-house. C57BL/6 *Mr1*$^{-/-}$ mice were kindly provided by James McCluskey (Melbourne University, Melbourne, Australia; ref. 5). C57BL/6 *IL17A*$^{-/-}$ mice were provided by Geoffrey R. Hill (QIMR Berghofer Medical Research Institute, Herston, Australia; ref. 56). *Tcrd*$^{-/-}$ mice were provided by Ian Frazer (The University of Queensland, Brisbane, Australia). *Rag2cγ*$^{-/-}$ mice were generated at QIMR Berghofer Medical Research Institute by crossing *Rag2*$^{-/-}$ mice with *IL2Rγ*$^{-/-}$ mice (57). WT and *Mr1*$^{-/-}$ mice were cohoused in the same cage for at least 4 weeks before experiment initiation unless specifically indicated. Age-matched mice were used in all experiments. All WT and gene-targeted mice used were between the ages of 6 and 14 weeks. All experiments were approved by the QIMR Berghofer Medical Research Institute Animal Ethics Committee.

Cell Culture

The mouse melanoma cell lines B16F10, LWT1, and SM1WT1 and the MCA1956 fibrosarcoma cell line were maintained as described previously (37, 44, 58). Anti-MR1 antibody-producing hybridoma cell lines (clone 26.5 IgG2a isotype and 8F2.F9 IgG1 isotype) were maintained in complete RPMI-1640 media containing 10% FBS, 1% L-glutamine, and 1% penicillin/streptomycin (6, 42). All cell lines were routinely tested for *Mycoplasma*, but cell line authentication was not routinely performed.

Antibodies and Reagents for In Vivo Experiments

Anti-CD8β (clone 53.5.8), anti-IFNγ (clone H22), and control IgG antibody (clone 1-1) were purchased from BioXCell or Leinco. Anti-asialoGM1 (ASGM1) was purchased from Wako Pure Chemicals. Anti-MR1 mAbs were purified from the supernatant of hybridoma cells by protein G affinity resin column (6, 42). The dose and schedule of antibody treatment are indicated in the figure legends. Biotinylated MR1–antigen monomer was conjugated with PE–streptavidin (BioLegend, catalog no. 5544061) to generate MR1 tetramers as described previously (7, 17, 18, 59). MAIT cell antigen 5-OP-RU was generated as described previously (8), whereas Ac-6-FP (60) was bought from Schircks Laboratories. Cell stimulation cocktail (PMA/ionomycin plus protein transport inhibitors) was purchased from Invitrogen Thermo Fisher Scientific (catalog no. 00-4975-93).

Tumor Models

The indicated numbers of B16F10 and LWT1 cells were injected intravenously into the tail vein of WT or gene-targeted female or male mice, respectively. In some experiments, B16F10 and LWT1 cells were treated with 5-OP-RU (100 nmol/L, 4 hours) or Ac-6-FP (10 μmol/L, 18 hours) or their respective DMSO or ddH_2O vehicle controls before injection. Cells with viability greater than 90% were used in the experiments. Lungs were harvested on day 14, and surface tumor nodules were counted under a dissection microscope as previously described (37, 39). For therapy experiments, anti-MR1 or cIg (clone 1-1, Leinco) were injected intraperitoneally into mice at the dose and schedule indicated in the figure legends. SM1WT1 or MCA1956 (both 1×10^6) tumor cells were injected subcutaneously into WT or gene-targeted male or female mice, respectively, prior to treatment with cIg or anti-MR1 at time points indicated in the figure legends. For MCA-induced fibrosarcoma, WT and *Mr1*$^{-/-}$ male mice were injected subcutaneously in the hind flank with MCA (Sigma-Aldrich) in 100 μL of corn oil as described previously (37, 61) with the doses indicated in the figure legends. For established tumor MCA experiments, mice were treated intraperitoneally with cIg or anti-MR1 from the second palpable tumor measurement twice a week for 6 weeks as indicated in the figure legend. Mice were monitored for fibrosarcoma development over 200 to 250 days. Tumor sizes were determined by caliper square measurements of two perpendicular diameters with data represented as mean ± SEM (mm^2) for each group.

BM Transplantation and Reconstitution

BM cells were obtained from the femurs of donor C57BL/6 WT (PTPRCA and CD45.1$^+$) mice and *Mr1*$^{-/-}$ (C57BL/6 and CD45.2$^+$) mice. Two doses of 5.5 Gy of whole-body irradiation were administered to recipient WT and *Mr1*$^{-/-}$ mice at 4-hour intervals. Recipient

mice were injected intravenously with 5×10^6 BM cells/mouse after irradiation. Mice were provided with water containing neomycin for 4 weeks. Ten weeks after BM transplantation, mice were eye-bled and immune cells were analyzed by flow cytometry using congenic CD45.1 and CD45.2 markers to assess immune cell reconstitution before mice were used experimentally.

Flow Cytometry

Naïve or tumor-bearing lungs or subcutaneous tumor single-cell suspensions were generated as described previously (37) and incubated with anti-CD16/32 (2.4G2) to block Fc receptors on ice prior to surface staining with the antibodies. The following antibodies were used for FACS analysis: anti-CD45.2 (104), anti-TCRβ (H57-597), anti-NK1.1 (PK136), anti-NKp46 (29A1.4), anti-CD45R (B220, RA3-6B2), anti-F4/80 (BM8), anti-CD69 (H1.2F3; all from BioLegend, eBioscience), and MR1 tetramers. For intracellular cytokine staining, cells were surface-stained as described above and then fixed and permeabilized with a Cytofix/Cytoperm Kit (BD Biosciences) followed by staining with anti-IFNγ (XMG1.2), anti-TNF (MP6-XT22), anti-IL17A (TC11-18H10.1), or isotype (eBio299Arm) antibody (all from BioLegend). All data were collected on a Fortessa 4 Flow Cytometer (BD Biosciences) and analyzed with FlowJo v10 Software (TreeStar, Inc.).

Ex Vivo *Immune Cell Cytokine and Degranulation Assay*

Single-cell suspensions from naïve or tumor-bearing lungs or subcutaneous tumors of the indicated groups were incubated in a 96-well U-bottom plate in complete RPMI-1640 media. Cells were incubated in the presence or absence of cell stimulation cocktail (PMA/ionomycin plus protein transport inhibitors; 1,000 times dilution) for 3 to 4 hours as indicated. Cells were then stained for surface markers and intracellular cytokine production. A CD107a staining assay was used to assess the degranulation status of immune cells. Briefly, anti-CD107a (1D4B, BioLegend) antibody was added to single-cell suspensions during the stimulation period before these cells were surface-stained and analyzed by flow cytometry.

MAIT Cell Expansion and Sorting

MAIT cells were expanded using the protocol described by Varelias and colleagues (24). Briefly, spleens from WT, *Tcrd*$^{-/-}$, or *Il17a*$^{-/-}$ mice were mashed through a 40-μm cell strainer and lysed with ACK buffer to remove red blood cells. Splenocytes were cultured in complete RPMI-1640 media containing 50 ng/mL (250 U/mL) mouse IL2 (PeproTech; catalog no. 212-12) and 100 nmol/L 5-OP-RU. On days 6 and 7, cells were harvested for sorting. Anti-CD16/32 (2.4G2) to block Fc receptors were added to the single-cell suspension before staining with biotin-B220 antibody (clone RA3-6B2, Miltenyi Biotec; catalog no. 130-101-928) followed by Streptavidin MicroBeads (Miltenyi Biotec; catalog no. 130-048-101) to deplete B220$^+$ cells by MACS. The enriched splenocytes were stained with an antibody cocktail and MAIT cells (B220$^-$ F4/80$^-$ CD45.2$^+$ TCRβ$^+$ MR1–5-OP-RU tetramer$^+$) and non-MAIT cells (B220$^-$ F4/80$^-$ CD45.2$^+$ TCRβ$^+$ MR1–5-OP-RU tetramer$^-$) were sorted on an Aria II/Aria III (see gating strategy in Supplementary Fig. S1A). MAIT cells of 85% to 95% purity were used in subsequent experiments.

MR1 Knockout with CRISPR/Cas9 in B16F10 Cells

MR1 was knocked out in B16F10 cells using the CRISPR/Cas9 system. Three mouse *Mr1* sgRNAs (Supplementary Table S1) were designed on the CHOPCHOP website (http://chopchop.cbu.uib.no/). Briefly, the three *Mr1* sgRNAs were subcloned into PX459 vectors (Addgene; catalog no. 62988), respectively, following the one-step protocol as described by Ran and colleagues (62). PX459 plasmids containing *Mr1* sgRNA and pRp GFP-expressing plasmids were cotransfected into B16F10 cells using FuGENE6 Transfection Reagent (Promega; catalog no. E2691). On the following day, cells were cultured in media containing 1 μg/mL puromycin (Sigma-Aldrich) for 2 days. The GFP$^+$ cells were sorted using the FACSAria III cell sorter (BD Biosciences) into 96-well flat-bottom plate (1 cell/well) to obtain monoclonal B16F10-MR1^{KO} cell lines. MR1 knockout in B16F10 cells was verified by determining MR1 surface expression after 100 nmol/L 5-OP-RU stimulation for 4 hours as described above.

MR1 Reexpression in B16F10-MR1^{KO} Cells

B16F10-MR1^{KO} cells were transfected with MR1-expressing pCMV6-AC-GFP plasmid (OriGene; catalog no. MG205125) or empty control plasmid (OriGene; catalog no. PS100010) using FuGENE6 Transfection Reagent. Two days later, cells were cultured in media containing 500 μg/mL Geneticin Selective Antibiotic (G418 Sulfate; Thermo Fisher Scientific, catalog no. 10131035) for 2 weeks. GFP$^+$ cells were sorted to obtain a stable cell line. MR1 expression was verified by determining MR1 surface expression after 100 nmol/L 5-OP-RU stimulation for 4 hours as described above.

Statistical Analysis

GraphPad Prism software was used for statistical analysis. One-way ANOVA with Tukey *post hoc* test was used for multiple comparisons, Mann–Whitney test for two-group comparison, and log-rank (Mantel–Cox) test for mouse survival. Differences between groups were considered to be statistically significant where the P value was less than 0.05.

Disclosure of Potential Conflicts of Interest

M.J.S is funded by research agreements from Bristol-Myers Squibb and Tizona Therapeutics and has an advisory board role for Tizona Therapeutics and Compass Therapeutics. L.L., A.C., and D.P.F are named inventors on a patent application (PCT/AU2013/000742, WO2014005194) and J.Y.W.M., L.L., A.C., Z.C., and D.P.F are named inventors on another patent application (PCT/AU2015/050148, WO2015149130) involving MR1 ligands for MR1-restricted MAIT cells owned by University of Queensland, Monash University, and University of Melbourne. No potential conflicts of interest were disclosed by the other authors.

Authors' Contributions

Conception and design: J. Yan, M.J. Smyth, M.W.L. Teng
Development of methodology: J. Yan, S. Allen, M.J. Smyth
Acquisition of data (provided animals, acquired and managed patients, provided facilities, etc.): J. Yan, I. Das, J.Y.W. Mak, B.S. Meehan, A.J. Corbett, A. Varelias, M.J. Smyth
Analysis and interpretation of data (e.g., statistical analysis, biostatistics, computational analysis): J. Yan, I. Das, A. Varelias, M.J. Smyth, M.W.L. Teng
Writing, review, and/or revision of the manuscript: J. Yan, E. McDonald, J.Y.W. Mak, D.P. Fairlie, A.J. Corbett, A. Varelias, M.J. Smyth, M.W.L. Teng
Administrative, technical, or material support (i.e., reporting or organizing data, constructing databases): J. Yan, S. Allen, E. McDonald, L. Liu, D.P. Fairlie, Z. Chen, M.W.L. Teng
Study supervision: M.W.L. Teng

Acknowledgments

The authors thank Liam Town, Kate Elder, Brodie Quine, and Gabrielle Kelly for breeding and genotyping of mice throughout this study. We would also like to thank Glen Boyle and Frank Vari for kindly providing human tumor cell lines, and Sebastien Jacquelin and Xian Yang Li for CRISPR/Cas9 technical assistance. We would also like to thank Dillon Corvino, Venkateswar Addala, and John Stagg for their intellectual input and helpful discussions. M.J. Smyth was supported by an NH&MRC Research Fellowship (1078671).

M.W.L. Teng was supported by an NH&MRC CDF Fellowship (1159655). J. Yan was supported by a University of Queensland International Scholarship co-funded by QIMR Berghofer. A.J. Corbett is supported by an ARC Future Fellowship (FT160100083). D.P. Fairlie is supported by an NH&MRC Senior Principal Research Fellowship (1117017) and an ARC Centre of Excellence grant (CE140100011).

The costs of publication of this article were defrayed in part by the payment of page charges. This article must therefore be hereby marked *advertisement* in accordance with 18 U.S.C. Section 1734 solely to indicate this fact.

Received May 18, 2019; revised September 9, 2019; accepted October 18, 2019; published first December 11, 2019.

REFERENCES

1. Fridman WH, Pages F, Sautes-Fridman C, Galon J. The immune contexture in human tumours: impact on clinical outcome. Nat Rev Cancer 2012;12:298–306.
2. Godfrey DI, Le Nours J, Andrews DM, Uldrich AP, Rossjohn J. Unconventional T cell targets for cancer immunotherapy. Immunity 2018;48:453–73.
3. Tilloy F, Treiner E, Park SH, Garcia C, Lemonnier F, de la Salle H, et al. An invariant T cell receptor alpha chain defines a novel TAP-independent major histocompatibility complex class Ib-restricted alpha/beta T cell subpopulation in mammals. J Exp Med 1999;189:1907–21.
4. Le Bourhis L, Guerri L, Dusseaux M, Martin E, Soudais C, Lantz O. Mucosal-associated invariant T cells: unconventional development and function. Trends Immunol 2011;32:212–8.
5. Treiner E, Duban L, Bahram S, Radosavljevic M, Wanner V, Tilloy F, et al. Selection of evolutionarily conserved mucosal-associated invariant T cells by MR1. Nature 2003;422:164–9.
6. Huang S, Gilfillan S, Cella M, Miley MJ, Lantz O, Lybarger L, et al. Evidence for MR1 antigen presentation to mucosal-associated invariant T cells. J Biol Chem 2005;280:21183–93.
7. Corbett AJ, Eckle SB, Birkinshaw RW, Liu L, Patel O, Mahony J, et al. T-cell activation by transitory neo-antigens derived from distinct microbial pathways. Nature 2014;509:361–5.
8. Mak JY, Xu W, Reid RC, Corbett AJ, Meehan BS, Wang H, et al. Stabilizing short-lived Schiff base derivatives of 5-aminouracils that activate mucosal-associated invariant T cells. Nat Commun 2017;8:14599.
9. Patel O, Kjer-Nielsen L, Le Nours J, Eckle SB, Birkinshaw R, Beddoe T, et al. Recognition of vitamin B metabolites by mucosal-associated invariant T cells. Nat Commun 2013;4:2142.
10. Eckle SB, Birkinshaw RW, Kostenko L, Corbett AJ, McWilliam HE, Reantragoon R, et al. A molecular basis underpinning the T cell receptor heterogeneity of mucosal-associated invariant T cells. J Exp Med 2014;211:1585–600.
11. Kjer-Nielsen L, Patel O, Corbett AJ, Le Nours J, Meehan B, Liu L, et al. MR1 presents microbial vitamin B metabolites to MAIT cells. Nature 2012;491:717–23.
12. Keller AN, Eckle SB, Xu W, Liu L, Hughes VA, Mak JY, et al. Drugs and drug-like molecules can modulate the function of mucosal-associated invariant T cells. Nat Immunol 2017;18:402–11.
13. Eckle SB, Corbett AJ, Keller AN, Chen Z, Godfrey DI, Liu L, et al. Recognition of vitamin B precursors and byproducts by mucosal associated invariant T cells. J Biol Chem 2015;290:30204–11.
14. Okada S, Markle JG, Deenick EK, Mele F, Averbuch D, Lagos M, et al. Immunodeficiencies. Impairment of immunity to *Candida* and *Mycobacterium* in humans with bi-allelic RORC mutations. Science 2015;349:606–13.
15. Dusseaux M, Martin E, Serriari N, Peguillet I, Premel V, Louis D, et al. Human MAIT cells are xenobiotic-resistant, tissue-targeted, CD161hi IL-17-secreting T cells. Blood 2011;117:1250–9.
16. Tang XZ, Jo J, Tan AT, Sandalova E, Chia A, Tan KC, et al. IL-7 licenses activation of human liver intrasinusoidal mucosal-associated invariant T cells. J Immunol 2013;190:3142–52.
17. Reantragoon R, Corbett AJ, Sakala IG, Gherardin NA, Furness JB, Chen Z, et al. Antigen-loaded MR1 tetramers define T cell receptor heterogeneity in mucosal-associated invariant T cells. J Exp Med 2013;210:2305–20.
18. Rahimpour A, Koay HF, Enders A, Clanchy R, Eckle SB, Meehan B, et al. Identification of phenotypically and functionally heterogeneous mouse mucosal-associated invariant T cells using MR1 tetramers. J Exp Med 2015;212:1095–108.
19. Chua WJ, Truscott SM, Eickhoff CS, Blazevic A, Hoft DF, Hansen TH. Polyclonal mucosa-associated invariant T cells have unique innate functions in bacterial infection. Infect Immun 2012;80:3256–67.
20. Ussher JE, Bilton M, Attwod E, Shadwell J, Richardson R, de Lara C, et al. CD161++CD8+T cells, including the MAIT cell subset, are specifically activated by IL-12+IL-18 in a TCR-independent manner. Eur J Immunol 2014;44:195–203.
21. Meermeier EW, Harriff MJ, Karamooz E, Lewinsohn DM. MAIT cells and microbial immunity. Immunol Cell Biol 2018;96:607–17.
22. van Wilgenburg B, Scherwitzl I, Hutchinson EC, Leng T, Kurioka A, Kulicke C, et al. MAIT cells are activated during human viral infections. Nat Commun 2016;7:11653.
23. Chen Z, Wang H, D'Souza C, Sun S, Kostenko L, Eckle SB, et al. Mucosal-associated invariant T-cell activation and accumulation after in vivo infection depends on microbial riboflavin synthesis and co-stimulatory signals. Mucosal Immunol 2017;10:58–68.
24. Varelias A, Bunting MD, Ormerod KL, Koyama M, Olver SD, Straube J, et al. Recipient mucosal-associated invariant T cells control GVHD within the colon. J Clin Invest 2018;128:1919–36.
25. Koay HF, Gherardin NA, Enders A, Loh L, Mackay LK, Almeida CF, et al. A three-stage intrathymic development pathway for the mucosal-associated invariant T cell lineage. Nat Immunol 2016;17:1300–11.
26. Martin E, Treiner E, Duban L, Guerri L, Laude H, Toly C, et al. Stepwise development of MAIT cells in mouse and human. PLoS Biol 2009;7:e54.
27. D'Souza C, Chen Z, Corbett AJ. Revealing the protective and pathogenic potential of MAIT cells. Mol Immunol 2018;103:46–54.
28. Sundstrom P, Ahlmanner F, Akeus P, Sundquist M, Alsen S, Yrlid U, et al. Human mucosa-associated invariant T cells accumulate in colon adenocarcinomas but produce reduced amounts of IFN-γ. J Immunol 2015;195:3472–81.
29. Zabijak L, Attencourt C, Guignant C, Chatelain D, Marcelo P, Marolleau JP, et al. Increased tumor infiltration by mucosal-associated invariant T cells correlates with poor survival in colorectal cancer patients. Cancer Immunol Immunother 2015;64:1601–8.
30. Ling L, Lin Y, Zheng W, Hong S, Tang X, Zhao P, et al. Circulating and tumor-infiltrating mucosal associated invariant T (MAIT) cells in colorectal cancer patients. Sci Rep 2016;6:20358.
31. Won EJ, Ju JK, Cho YN, Jin HM, Park KJ, Kim TJ, et al. Clinical relevance of circulating mucosal-associated invariant T cell levels and their anti-cancer activity in patients with mucosal-associated cancer. Oncotarget 2016;7:76274–90.
32. Peterfalvi A, Gomori E, Magyarlaki T, Pal J, Banati M, Javorhazy A, et al. Invariant Valpha7.2-Jalpha33 TCR is expressed in human kidney and brain tumors indicating infiltration by mucosal-associated invariant T (MAIT) cells. Int Immunol 2008;20:1517–25.
33. Zheng C, Zheng L, Yoo JK, Guo H, Zhang Y, Guo X, et al. Landscape of infiltrating T cells in liver cancer revealed by single-cell sequencing. Cell 2017;169:1342–56.
34. Gherardin NA, Loh L, Admojo L, Davenport AJ, Richardson K, Rogers A, et al. Enumeration, functional responses and cytotoxic capacity of MAIT cells in newly diagnosed and relapsed multiple myeloma. Sci Rep 2018;8:4159.
35. Favreau M, Venken K, Faict S, Maes K, De Veirman K, De Bruyne E, et al. Both mucosal-associated invariant and natural killer T-cell deficiency in multiple myeloma can be countered by PD-1 inhibition. Haematologica 2017;102:e266–e70.
36. Shaler CR, Tun-Abraham ME, Skaro AI, Khazaie K, Corbett AJ, Mele T, et al. Mucosa-associated invariant T cells infiltrate hepatic metastases in patients with colorectal carcinoma but are rendered dysfunctional within and adjacent to tumor microenvironment. Cancer Immunol Immunother 2017;66:1563–75.

37. Blake SJ, Stannard K, Liu J, Allen S, Yong MC, Mittal D, et al. Suppression of metastases using a new lymphocyte checkpoint target for cancer immunotherapy. Cancer Discov 2016;6:446–59.
38. Smyth MJ, Thia KY, Street SE, Cretney E, Trapani JA, Taniguchi M, et al. Differential tumor surveillance by natural killer (NK) and NKT cells. J Exp Med 2000;191:661–8.
39. Yan J, Allen S, Vijayan D, Li XY, Harjunpaa H, Takeda K, et al. Experimental lung metastases in mice are more effectively inhibited by blockade of IL23R than IL23. Cancer Immunol Res 2018;6:978–87.
40. Lamichhane R, Ussher JE. Expression and trafficking of MR1. Immunology 2017;151:270–9.
41. McWilliam HE, Eckle SB, Theodossis A, Liu L, Chen Z, Wubben JM, et al. The intracellular pathway for the presentation of vitamin B-related antigens by the antigen-presenting molecule MR1. Nat Immunol 2016;17:531–7.
42. Chua WJ, Kim S, Myers N, Huang S, Yu L, Fremont DH, et al. Endogenous MHC-related protein 1 is transiently expressed on the plasma membrane in a conformation that activates mucosal-associated invariant T cells. J Immunol 2011;186:4744–50.
43. Wang H, D'Souza C, Lim XY, Kostenko L, Pediongco TJ, Eckle SBG, et al. MAIT cells protect against pulmonary *Legionella longbeachae* infection. Nat Commun 2018;9:3350.
44. Mittal D, Lepletier A, Madore J, Aguilera AR, Stannard K, Blake SJ, et al. CD96 is an immune checkpoint that regulates $CD8^+$ T-cell antitumor function. Cancer Immunol Res 2019;7:559–71.
45. Ghiringhelli F, Menard C, Terme M, Flament C, Taieb J, Chaput N, et al. CD4+CD25+ regulatory T cells inhibit natural killer cell functions in a transforming growth factor-beta-dependent manner. J Exp Med 2005;202:1075–85.
46. Smyth MJ, Teng MW, Swann J, Kyparissoudis K, Godfrey DI, Hayakawa Y. CD4+CD25+ T regulatory cells suppress NK cell-mediated immunotherapy of cancer. J Immunol 2006;176:1582–7.
47. Ghiringhelli F, Menard C, Martin F, Zitvogel L. The role of regulatory T cells in the control of natural killer cells: relevance during tumor progression. Immunol Rev 2006;214:229–38.
48. Liu C, Yu S, Kappes J, Wang J, Grizzle WE, Zinn KR, et al. Expansion of spleen myeloid suppressor cells represses NK cell cytotoxicity in tumor-bearing host. Blood 2007;109:4336–42.
49. Cekic C, Day YJ, Sag D, Linden J. Myeloid expression of adenosine A2A receptor suppresses T and NK cell responses in the solid tumor microenvironment. Cancer Res 2014;74:7250–9.
50. Mao Y, Sarhan D, Steven A, Seliger B, Kiessling R, Lundqvist A. Inhibition of tumor-derived prostaglandin-e2 blocks the induction of myeloid-derived suppressor cells and recovers natural killer cell activity. Clin Cancer Res 2014;20:4096–106.
51. Stiff A, Trikha P, Mundy-Bosse B, McMichael E, Mace TA, Benner B, et al. Nitric oxide production by myeloid-derived suppressor cells plays a role in impairing fc receptor-mediated natural killer cell function. Clin Cancer Res 2018;24:1891–904.
52. Guillerey C, Huntington ND, Smyth MJ. Targeting natural killer cells in cancer immunotherapy. Nat Immunol 2016;17:1025–36.
53. Dickson RP, Erb-Downward JR, Martinez FJ, Huffnagle GB. The microbiome and the respiratory tract. Annu Rev Physiol 2016;78:481–504.
54. Jin C, Lagoudas GK, Zhao C, Bullman S, Bhutkar A, Hu B, et al. Commensal microbiota promote lung cancer development via γδ T cells. Cell 2019;176:998–1013.
55. Legoux F, Bellet D, Daviaud C, El Morr Y, Darbois A, Niort K, et al. Microbial metabolites control the thymic development of mucosal-associated invariant T cells. Science 2019;366:494–9.
56. Nakae S, Komiyama Y, Nambu A, Sudo K, Iwase M, Homma I, et al. Antigen-specific T cell sensitization is impaired in IL-17-deficient mice, causing suppression of allergic cellular and humoral responses. Immunity 2002;17:375–87.
57. Chan CJ, Martinet L, Gilfillan S, Souza-Fonseca-Guimaraes F, Chow MT, Town L, et al. The receptors CD96 and CD226 oppose each other in the regulation of natural killer cell functions. Nat Immunol 2014;15:431–8.
58. Ferrari de Andrade L, Ngiow SF, Stannard K, Rusakiewicz S, Kalimutho M, Khanna KK, et al. Natural killer cells are essential for the ability of BRAF inhibitors to control BRAFV600E-mutant metastatic melanoma. Cancer Res 2014;74:7298–308.
59. Sakala IG, Kjer-Nielsen L, Eickhoff CS, Wang X, Blazevic A, Liu L, et al. Functional heterogeneity and antimycobacterial effects of mouse mucosal-associated invariant T cells specific for riboflavin metabolites. J Immunol 2015;195:587–601.
60. Freisleben A, Schieberle P, Rychlik M. Syntheses of labeled vitamers of folic acid to be used as internal standards in stable isotope dilution assays. J Agric Food Chem 2002;50:4760–8.
61. Swann JB, Hayakawa Y, Zerafa N, Sheehan KC, Scott B, Schreiber RD, et al. Type I IFN contributes to NK cell homeostasis, activation, and antitumor function. J Immunol 2007;178:7540–9.
62. Ran FA, Hsu PD, Wright J, Agarwala V, Scott DA, Zhang F. Genome engineering using the CRISPR-Cas9 system. Nat Protoc 2013;8:2281–308.

Published OnlineFirst December 11, 2019; DOI: 10.1158/2159-8290.CD-19-0569

AACR American Association for Cancer Research

CANCER DISCOVERY

MAIT Cells Promote Tumor Initiation, Growth, and Metastases via Tumor MR1

Juming Yan, Stacey Allen, Elizabeth McDonald, et al.

Cancer Discov 2020;10:124-141. Published OnlineFirst December 11, 2019.